Science Translational Medicine
AAAS

Supplementary Materials for

Enhancing GAT-3 in thalamic astrocytes promotes resilience to brain injury in rodents

Frances S. Cho *et al.*

Corresponding author: Jeanne T. Paz, jeanne.paz@gladstone.ucsf.edu

Sci. Transl. Med. **14**, eabj4310 (2022)
DOI: 10.1126/scitranslmed.abj4310

The PDF file includes:

Materials and Methods
Figs. S1 to S12
Tables S1 to S10

Other Supplementary Material for this manuscript includes the following:

Data files S1 and S2
MDAR Reproducibility Checklist

Materials and Methods

Animals

Male mice were used for all experiments, and ages ranged between postnatal days 28-300. C57BL6J mice were purchased from the Jackson Laboratory (Jax Strain No. 000664). Aldh1l1-tdTomato mice were bred by A.V.M. Floxed *Gabrd* ($Gabrd^{Fl/Fl}$) mice (Jax Strain No. 023836) were a gift from Dr. Jamie Maguire (Tufts University).

Fluorescence-activated cell sorting (FACS) of reactive astrocytes

Three weeks after unilateral injection of AAV2/5-Gfa104-eGFP into the VB thalamus, Aldh1l1-tdTomato mice were anesthetized with isoflurane and perfused with ice-cold HBSS-Ca/Mg-free supplemented with Hepes and glucose *(78)*. Ventrobasal (VB) thalami were microdissected into ipsilateral and contralateral samples under a dissecting microscope and dissociated with papain 20 U/ml (Worthington) for 45 minutes at 34 ^{o}C as previously described *(79)*. A 22% Percoll gradient was run to deplete myelin and subsequently the single cell suspension was incubated with following antibodies in HBSS-Ca/Mg-free supplemented with Hepes, glucose and EDTA *(78)* on ice for 30 minutes: CD11b APC, CD45 Percp-Cy5.5 and Ly-6C APC/Cy7 (eBioscience/Biolegend). Samples were incubated with DAPI and FACS was performed on a BD Aria3 to collect purified astrocyte populations (fig. S2). Ipsilateral reactive astrocytes transduced by AAV-eGFP were gated as $DAPI^{neg}CD11b^{neg}tdTomato^{pos}eGFP^{pos}$, and contralateral "healthy" astrocytes were gated as $DAPI^{neg}CD11b^{neg}tdTomato^{pos}eGFP^{neg}$. DAPI was used for live/dead exclusion and CD11b to exclude microglia. Cells were collected in RLT+ (Qiagen) and stored at -80 ^{o}C.

qPCR and RNA sequencing of FACS-astrocytes

RNA was isolated from FACS-astrocytes with the Rneasy Plus Micro kit (Qiagen) and quality and concentration were assessed with the Agilent RNA 6000 Pico kit on a Bioanalyzer (Agilent). For qPCR analysis, RNA was reverse transcribed using the high capacity cDNA reverse transcription kit (Applied Biosystems) and qPCR was run on a 7900HT Fast Real-Time PCR System (Applied Biosystems) using Fast SYBR Green Master Mix (Applied Biosystems) and the following primers: *Slc6a11* -FW: CGGCTGGGTATATGGAAGCA -RV: ACGACTTTCCAGCACCACTT; *Aldh1l1* -FW: CTTCATAGGCGGCGAGTTTGTG -RV: CGCCTTGTCAACATCACTCACC; GFP -FW: AAGTTCATCTGCACCACCG -RV: TCCTTGAAGAAGATGGTGCG. CT cycles were analyzed with 7900 SDS v2.4 software (Applied Biosystems) and $2^{-\Delta CT}$ method was used to determine expression. For RNA sequencing, cDNA and libraries were made using the Ovation RNA-Seq System V2 kit (NuGen). Quality was measured by Agilent High Sensitivity DNA kit on a Bioanalyzer (Agilent) and quantified by qPCR. Libraries were pooled and RNA sequencing was performed on an Illumina HiSeq 4000 with single end (SE50) sequencing. Around 60-80 million reads were sequenced per sample.

Transcriptomic analysis of bulk RNA-Seq

Bioinformatic analysis of bulk RNA-Seq of FACS-isolated thalamic astrocytes was performed as previously described *(74)*. FastQC was used to assess read quality. Reads were pseudo aligned to the *Mus musculus* transcriptome (cDNA, Ensembl GRCm38) using Kallisto (version 0.44.0) with kmer size 31 and bootstraps set to 100. Kallisto generated transcript per million (TPM) and transcript abundance values that were loaded into R (The R Foundation) using Tximport. TPM values per gene were generated from the per isoform values. DESeq2 package was used to determine differentially expressed genes, where genes with an adjusted p-value < 0.05 were considered significantly differentially expressed. Heatmaps were made using the ComplexHeatmap package.

Immunohistochemistry of mouse brain tissue

Mice were anesthetized with a lethal dose of FatalPlus and perfused with ice-cold 4% paraformaldehyde in phosphate buffered saline (PBS). All brains were visually assessed for signs of gross damage before sectioning. Serial coronal sections (50 μm) were cut on a sliding microtome (Leica SM2000R), selecting sections near the site of injection (Bregma –1.65 mm). After immunohistochemical protocols, sections were mounted in an antifade medium (Vectashield) and imaged using fluorescence microscopy (Keyence BZ-9000) or confocal microscopy (Zeiss LSM880). Brain sections were visually assessed for signs of gross damage on the side which received a unilateral manipulation (with the contralateral hemibrain used as a control).

To verify the location and extent of thalamic astrogliosis, sections were immunostained with the following antibodies: glial fibrillary acidic protein (GFAP) (1:1000; host species chicken; Abcam ab4674; RRID:AB_304558), GFP (1:1000; host species goat; Abcam ab6673; RRID:AB_305643), GAT-3 (1:200; host species rabbit; Abcam ab431; RRID:AB_304437); mCherry (1:500; host species rabbit; Abcam ab167453; RRID:AB_2571870); and the following secondary antibodies (1:500): donkey anti-chicken AF594 (Jackson ImmunoResearch Labs #703-585-155; RRID:AB_2340377), donkey anti-goat AF488 (Abcam ab150129; RRID:AB_2687506), goat anti-rabbit AF594 (Thermo Fisher #A-11037; RRID:AB_2534095). Sections were blocked in normal donkey or goat serum (Jackson ImmunoResearch Labs #017-000-121 (RRID:AB_2337258) & #005-000-121 (RRID:AB_2336990). Free-floating sections were washed in PBS (3 x 10 min), permeabilized with 0.5% Triton in PBS (PBST-0.5%), washed in PBST-0.05%, and blocked in 10% normal goat or donkey serum (diluted in PBST-0.05%) for 1 hour. Sections were incubated with primary antibodies in 3% normal goat or donkey serum, overnight at 4 °C. Following 3x10 min washes in PBST-0.05%, the sections were incubated with secondary antibodies for 1-2 hr at room temperature. Sections were then washed in PBST and PBS, mounted onto glass slides, and coverslipped with Vectashield antifade reagent (Vector Laboratories, H-1000), and stored at 4 °C.

To verify deletion of the δ-subunit in the $Gabrd^{Fl/Fl}$ mice, we performed DAB-based IHC on free-floating sections (50 μm). Endogenous peroxidase activity was quenched for 30 min in 1% v/v hydrogen peroxide in 30% ethanol. The blocking of nonspecific binding was achieved with 10% normal goat serum (NGS) for 1 hour at room temperature (RT). The antibody against $GABA_AR$ δ-subunit (1:500; host species rabbit, polyclonal, MilliporeSigma AB9752; RRID:AB_672966) was dissolved in 5% NGS and the sections were incubated in RT overnight. For horseradish peroxidase (HRP) staining, sections were incubated with Mach 2 anti-rabbit HRP polymer (Biocare Medical, RHRP520) for 1 hour at RT. The activity of HRP was visualized with a commercially available kit for 3,3′-diaminobenzidine (DAB) peroxide substrate (Vector Laboratories, SK-4100; RRID:AB_2336382). Sections were washed in PBTS-0.1%. between each immunohistochemical step. Finally, immunostained sections were mounted on gelatinized slides, dehydrated in alcohol and xylene and cover-slipped with Cytoseal (ThermoFisher Scientific, 8310-16). Control sections were processed without primary antibodies, and no immunostaining was observed under these conditions.

For morphological characterization of astrocytes, we performed stereotaxic injections of AAV-eGFP into VB thalamus of two-month-old EAAT2-tdTomato mice. After three weeks, mice were anesthetized with isoflurane, and perfused with ice-cold PBS followed by ice-cold 4% PFA. The brains were collected and post-fixed in 4% PFA overnight at 4 °C. Subsequently, brains were placed in 30% sucrose solution in PBS for two consecutive nights. Brains were frozen and sectioned (60 μm) on a Cryostat (Leica). For immunohistochemistry, sections were treated with 0.01 M citrate buffer pH 6.0 for 2 min at 95 °C for antigen retrieval, blocked for 1 hour at room temperature with 5% normal goat serum (NGS) in PBS with 0.25% Triton X-100. Primary antibody staining was

done overnight at 4 °C with rat anti-GFAP (1:1000, Invitrogen, 13-0300), chicken anti-GFP (1:1000, Aves Labs, GFP-1020) and rabbit anti-RFP/DsRed (1:1000, Living Colors DsRed Polyclonal Antibody, Clontech, 632496) in PBS with 2% NGS and 0.25% Triton X-100. For secondary antibody staining, sections were incubated with goat anti-rat AF647, goat anti-chicken AF488, goat anti-rabbit AF555 (all at 1:400, from Thermo Fisher Scientific) in PBS with 2% NGS and 0.25 Triton X-100 for 1.5 hours at RT. Sections were embedded on slides in DAPI Fluoromount-G (SouthernBiotech, 0100-20). Z-stacks with a step size of 1 µm at 40x magnification from the VB thalamus were collected on a Zeiss LSM880. Using Fiji (ImageJ), maximum intensity images were generated and the EAAT2-tdTomato channel images were used to create binary, thresholded images for morphology analysis. Sholl analysis *(37)* was performed in Fiji (ImageJ) on astrocytes from the binary images with a step size of 1 µm.

Quantification of mouse immunohistochemical data

Images were obtained with the Keyence fluorescence microscope, using BZ Viewer and BZ Analyzer software. Image quantification was performed in ImageJ (U.S. National Institutes of Health). For image quantification (10x magnification), we chose 2-4 sections for each mouse between -1.3 mm and -1.6 mm posterior from Bregma *(76)*. Regions of interest (ROI) were selected based on the mouse brain atlas *(76)* for both hemispheres (ipsilateral and contralateral to site of injection and/or injury). Fluorescence intensity was obtained from 8-bit images as the sum of the values of the pixels in each ROI (using "Raw Integrated Density" in ImageJ), and normalized by each ROI area. Normalized fluorescence intensity of the ipsilateral side was then divided by the normalized fluorescence intensity of the contralateral side to obtain the fluorescence intensity ratio of one section. For quantification in the thalamus, thalamic nuclei include the ventroposterior medial, ventroposterior lateral, ventrolateral, posterior medial, dorsal lateral geniculate, and lateral posterior nuclei, unless specified otherwise as in the case of quantification of the reticular thalamic nucleus). Quantification in the hippocampus included CA1, CA3, and dentate gyrus. Quantification in the somatosensory cortex included the S1 barrel field (S1BF) and S1 trunk (S1Tr). Quantification was performed in sections obtained along the AP axis in which all ROIs were visible. No exclusion criteria were applied.

Immunohistochemistry of human post-mortem brain tissue

The cases included in this study were obtained from the archives of the Amsterdam University Medical Centers. Brain samples (peri-lesional cortex and thalamus) were obtained from 4 patients who died after TBI and 3 patients who died after ischemic stroke. Control material was obtained at autopsy from 3 age-matched controls, without a history of seizures or other neurological diseases. All autopsies were performed within 24 h after death. Tissue was obtained and used in accordance with the Declaration of Helsinki and the Amsterdam UMC Research Code provided by the Medical Ethics Committee. All cases were reviewed independently by two neuropathologists. The clinical information of each patient is reported in table S1.

Human brain tissue was fixed in 10% buffered formalin and embedded in paraffin. Paraffin embedded tissue was sectioned at 5 µm, mounted on pre-coated glass slides (Star Frost, Waldemar Knittel) and processed for immunohistochemical staining. Sections were deparaffinated in xylene, rinsed in ethanol (100%, 95%, 70%) and incubated for 20 min in 0.3% hydrogen peroxide diluted in methanol. Antigen retrieval was performed using a pressure cooker in 0.01 M sodium citrate buffer (pH 6.0) at 120°C for 10 min. Slides were washed with PBS, pH 7.4) and incubated overnight with primary antibody (GAT-3, 1:450, ab431, Abcam) in PBS at 4°C. Sections were washed in PBS and then stained with a polymer-based peroxidase immunohistochemistry detection kit (Brightvision plus kit, ImmunoLogic,) according to the manufacturer's instructions. Staining was

performed using Bright 3,3'-diaminobenzidine (DAB) substrate solution (ImmunoLogic,). Reaction was stopped by washing in distilled water. Sections were counterstained with Haematoxylin-Mayer solution (Klinipath), dehydrated in alcohol and xylene and coverslipped. For double labeling, slides were incubated overnight with primary antibodies (GAT-3, 1:450 and GFAP (G-3893), 1:2000, Sigma-Aldrich) in PBS at 4°C. Afterwards, sections were incubated for two hours at room temperature with secondary antibodies, Alexa Fluor 568 donkey anti-mouse IgG (H+L) and Alexa Fluor 488 goat anti-rabbit IgG (H+L) (1:200, A10037 and A11008; Invitrogen), washed in PBS and coverslipped. Fluorescent microscopy was performed using a confocal microscope (SP8-X, Leica,) to acquire images of the perilesional cortex and thalamus from all autopsy post-mortem material. Fluorescence images were pseudocolored in ImageJ for visualization.

Quantification of immunoreactivity in human post-mortem tissue

Semi-quantitative analysis was performed by assessing GFAP immunoreactivity in the peri-lesional cortex and thalamus according to the following scale while blinded to condition (table S2): 1=sparse presence of cells with astrocyte-like morphology, of which the majority have a resting morphology; 2= moderate presence of cells with astrocyte-like morphology, with either resting or partially reactive morphology; 3= high presence of cells with astrocyte-like morphology, of which the majority have reactive morphology. Semi-quantitative analysis of GAT-3 immunoreactivity in the peri-lesional cortex and thalamus according to the following scale while blinded to condition (table S2): 0=absent, 1=sparse, 2=moderate, 3=dense staining. Quantification of GFAP immunofluorescence was performed by two investigators independently counting the number of GFAP-positive cells in ImageJ in a blinded manner (Fig. S11). Inclusion criteria for GFAP-positive cells included distinct immunopositive soma and at least one process protruding from the soma. For each image, the count of the two investigators was averaged. While blinded to condition, images were identified for exclusion if more than half of the image included fibrous white matter. Quantification of GAT-3 immunofluorescence was performed in perilesional cortex and thalamus using ImageJ (Fig. S11). Immunofluorescence images were converted to 8-bit grayscale then thresholded, such that the range of grayscale pixel values was set consistently across images of the same region, to obtain the mean gray value, as described in *(80)*. Per group, outliers were identified using ROUT method in GraphPad Prism.

Slice preparation for patch-clamp electrophysiology

Mice were euthanized with 4% isoflurane, then transcardially perfused with ice-cold sucrose cutting solution containing 234 mM sucrose, 2.5 mM KCl, 1.25 mM NaH_2PO_4, 10 mM $MgSO_4$, 0.5 mM $CaCl_2$, 26 mM $NaHCO_3$, and 11 mM glucose, equilibrated with 95% O_2 and 5% CO_2, pH 7.4. The thalamic slice preparation was performed as described *(43, 75)*. Horizontal thalamic slices containing the VB thalamus and nRT were cut at 250-µm (for patch-clamp electrophysiology) or 400-µm (for thalamic microcircuit studies) with a Leica VT1200 microtome (Leica Microsystems). Slices were incubated at 32 °C for 30 min, then at 24-26 °C for 1 hour, in artificial cerebrospinal fluid (aCSF) containing 126 mM NaCl, 2.5 mM KCl, 1.25 mM NaH_2PO_4, 1 mM $MgCl_2$, 2 mM $CaCl_2$, 26 mM $NaHCO_3$, and 10 mM glucose, equilibrated with 95% O_2 and 5% CO_2, pH 7.4. For tonic GABA recordings, slices were incubated and recorded in aCSF containing 126 mM NaCl, 26 mM $NaHCO_3$, 10 mM glucose, 2.5 mM KCl, 2 mM $MgCl_2$—$6H_2O$, 2 mM $CaCl_2$—$2H_2O$, and 1.25 mM NaH_2PO_4 *(81)*.

Analysis of electrophysiological properties of thalamic neurons

Tonic GABA recordings: Following GBZ (50 µM) bath application, neurons were recorded for at least 10 minutes. Tonic GABA current was defined as the shift in holding current due to GBZ

application, and marked by the stopping of phasic IPSCs. We obtained an average current at least 2 minutes pre- and post-stabilization of the shift in holding current. Currents were subtracted using Clampfit 10.5 (Molecular Devices, SCR_011323). Currents are presented without normalizing to cell capacitance, as capacitance did not differ between groups (table S3). All cellular physiology data were analyzed in a blinded manner.

Action potential properties: To characterize action potentials (APs) elicited by depolarizing intracellular current injections in thalamocortical neurons, we obtained the following parameters for the first AP which occurred at each neuron's rheobase (the amplitude of the first current step which elicited APs): the AP threshold, which was determined as the inflection point of the raw voltage trace immediately preceding the AP; the AP amplitude, defined as the voltage difference between the AP threshold and the maximal voltage of the AP; the AP duration, defined as the time between the AP threshold and the time at which membrane voltage returned to threshold; and the AP half-duration, defined as the duration between the half-maximal voltage in the depolarizing phase and the half-maximal voltage in the repolarizing phase.

T-Current biophysical properties: To assess steady-state inactivation properties of the T-current, the current-voltage response of each cell was fit with the Boltzmann function to determine the half-maximal voltage (V_{50}) *(12, 43)* (calculated using Origin Pro 9.0). All parameters (cell capacitance, maximal T-current area, maximal T-current amplitude, T-current density, maximal decay time constant, Boltzmann slope factor) were compared using unpaired t-tests or Mann-Whitney U tests (table S5).

Low-threshold spike (LTS) properties: To characterize the LTS-mediated rebound bursting, a custom MATLAB script was used to detect (1) V_H = membrane potential at the end of the hyperpolarizing current injection; (2) the threshold and latency to the LTS, indicated by the first deflection point during the period of depolarization (after the current injection) *(47)*; (3) AP firing rate during these rebound bursts, calculated by the number of APs divided by the duration between the first and last AP. FR was calculated only if there was more than 1 AP during the rebound burst. For each cell, we obtained the LTS parameters from the sweep in which the current injection hyperpolarized the cell the most.

Hyperpolarization-induced depolarizing sag potential properties: To characterize the depolarizing "sag" potential induced by hyperpolarization in thalamocortical neurons *(82)*, sag potentials were obtained as a function of the maximal hyperpolarized potential in response to a -150 pA intracellular current injection. The amplitude of the sag potential was calculated as the difference between the maximal hyperpolarized membrane potential and the membrane potential at the offset of the current injection. All recordings were performed at resting membrane potential.

Spontaneous synaptic currents: Frequency and kinetics of spontaneous excitatory and inhibitory synaptic currents were detected and analyzed using WDetecta (Huguenard Lab, Stanford University) as previously described *(12, 43)*. Spontaneous excitatory synaptic currents were obtained from the same samples presented in Fig. 3, B and D.

Electrophysiological recordings of extracellular thalamic oscillations and data analysis

Recordings: Horizontal slices (400 μm) containing somatosensory thalamus were placed in an interface chamber at 34 °C and superfused at a rate of 2 ml min^{-1} with oxygenated aCSF supplemented with 0.3 mM glutamine for cellular metabolic support *(43)*. Extracellular multi-unit activity (MUA) recordings were obtained with a linear 16-channel multi-electrode array (Neuronexus) that spanned the nRT and VB thalamic nuclei (Fig. 2C). MUA signals were amplified 10,000 times and band-pass filtered between 100 Hz and 6 kHz using the RZ5 from Tucker-Davis Technologies (TDT, SCR_006495). Position of recording array was visually checked for each recording to confirm position of electrodes in nRT and VB thalamic nuclei. Electrical stimuli were

delivered to the internal capsule with a bipolar tungsten microelectrodes (50–100 kΩ, FHC). The stimuli were 100 μs in duration, 50 V in amplitude, and delivered once every 30 s for 20 trials.

Comparison of thalamic circuit oscillations in thalamic slices: Extracellular spikes from multi-unit activity (MUA) were detected with custom MATLAB scripts (Huguenard Lab, Stanford University) by taking the first derivative of the signal and thresholding over baseline RMS values. Spikes were excluded if their waveform lasted longer than 2 ms. An experienced user confirmed parameter settings to optimize for all recordings. For automatic spike detection, the first three seconds of each trial was analyzed (Fig. 2, A, B, and E). As in previous literature, a burst of thalamic activity was defined as a cluster of ≥ 3 spikes occurring within 1 ms; and an oscillation as ≥ 2 bursts occurring within 1 second following stimulation, with an inter-burst interval of ≤ 1 second *(44)*. In Fig. 2D, we characterized the maximal evoked oscillatory activity by manually quantifying the number of evoked bursts and duration of oscillation that occurred in the 30 seconds following electrical stimulation (averaged across 20 trials for each slice), from the most responsive recording site of each slice.

Peri-stimulus time histograms (PSTH): Spikes were aligned to the stimulation onset and were used to calculate PSTH with a bin width of 10 ms (averaged across trials). Color axis represents the firing activity, scaled to the maximal number of spikes obtained in the slice (across all 16 recording sites and across all 20 trials).

Auto-correlation analysis: The spatiotemporal synchrony of oscillatory activity was determined by calculating the auto-correlation of the PSTH summed across the 16 recording sites in the thalamus and across all 20 trials for each slice (Fig. 2, A, B, and E). Note that only 9 of 16 sites are shown to aid visualization in Fig. 2 A and B. The PSTH and auto-correlation were calculated for 3 seconds after stimulation (excluding the first 150 ms which included the direct response), but only 1 second is shown in Fig. 2 for clarity. The auto-correlation was used to calculate the oscillatory index (O.I.) as previously described *(39, 44)*.

$$\text{O.I.} = 1 - \left[\frac{t_i}{\frac{p_i + p_{i+1}}{2}}\right]$$

where t_i= the i^{th} local minimum of the auto-correlation (trough) and p_i= the i^{th} local maximum of the auto-correlation (peak).

Surgical implantation of electrocorticography (EcoG) devices in mice

For short (up to 90 min-long recordings) *in vivo* electrophysiological recordings described in Figs. 4, 5, and fig. S6, electrocorticogram (EcoG) signal was acquired with a custom-made device containing multiple screws *(43)*. Cortical screws were implanted bilaterally in somatosensory cortex S1 (-0.5 mm posterior from Bregma, ± 3.5 mm lateral), in the right primary visual cortex V1 (-2.9 mm posterior from Bregma, ± 3.25 mm lateral), in the prefrontal cortex (+1.0 mm anterior from Bregma, 0 mm lateral), and a reference screw was implanted above the cerebellum (-0.5 mm posterior from Lambda, 0.5 mm lateral). Devices were fixed to the skull using dental cement.

For chronic, continuous 24/7 EcoG recordings (Fig. 6), mice were implanted with wireless telemetry devices as previously described *(10)* (PhysioTel HD-X02 Implants, Data Sciences International, Inc). Cortical screws were implanted bilaterally in somatosensory cortex S1 (-0.5 mm posterior from Bregma, $\pm$ 3.5 mm lateral) and a reference screw was implanted above the cerebellum (-0.5 mm posterior from Lambda, 0.5 mm lateral). The telemetry transponder was placed in the subcutaneous cavity above the shoulder.

Seizure susceptibility assay in mice implanted with multi-site ECoG electrodes

Following the induction of thalamic astrogliosis (3 weeks, 4 months and 7 months), seizure

susceptibility was determined by monitoring video and EcoG activity following i.p. administration of the pro-convulsant pentylenetetrazol (PTZ) (Tocris, #2687). At the beginning of each recording session, mice were briefly anesthetized with ~2% isoflurane prior to connecting the EcoG device to the headstage to minimize potential pain and/or strain to the implant site, and immediately returned to their home cage. For experiments reported in Fig. 4D and fig. S6B, mice were recorded for a 10-min period during which video and EcoG were monitored to ensure that mice regained mobility. Mice were then injected i.p. with PTZ and recorded with video and ECoG. Each PTZ recording trial lasted 45-90 min. PTZ assays and analysis were performed by investigators blinded to experimental group, and all groups within an experiment were subject to the same conditions.

PTZ is known to act on the thalamocortical circuit, even when administered systemically *(83)*. PTZ dose was optimized based on previously reported concentration ranges and pilot recordings for each cohort (in case there were slight variations depending on strain, age, cohorts). The dose selected was the lowest dose necessary to induce epileptiform discharges in mice with thalamic astrogliosis. Doses used in this study (ranging from 5 to 15 mg/kg) are typically sub-threshold for the same strain of mice in other studies *(84)*. Seizure susceptibility was also determined following i.p. administration of the pro-convulsant agent Kainic Acid (KA; 10 mg/kg) (Tocris, #0222). KA induced generalized convulsive seizures. Each mouse was recorded for 60 minutes following KA injection. Recordings and analysis were performed in a blinded manner.

Mouse cortical injury models and TBI seizure challenge assay

Stroke Model: Cortical photothrombotic stroke was induced in the somatosensory cortex as previously described *(12)*. Briefly, the light-sensitive dye Rose Bengal (40 mg/kg; Sigma-Aldrich #330000) dissolved in 0.9% saline was injected i.p. in isoflurane-anesthetized adult C57BL6 male mice. Immediately after RB injection, 2 minutes of 200 W illumination was delivered to the right somatosensory cortex using a 3-mm diameter fiber optic cable positioned directly on top of the skull (centered at -1 mm posterior from Bregma, 4 mm lateral). The optical system is designed to have an emission spectrum containing the *in vivo* absorption range of RB (maximum absorbance at 562 nm). Sham mice received identical anesthesia and scalp incision and RB but no illumination.

Traumatic Brain Injury Model: Controlled cortical impact (CCI) was induced in the somatosensory cortex as previously described *(10)*. Briefly, in isoflurane-anesthetized adult C57BL6 adult male mice, a 3-mm diameter craniotomy was performed over the right somatosensory cortex (centered at -1 mm posterior from Bregma, 3 mm lateral). A controlled cortical impact device equipped with a metal piston (Impact One Stereotaxic Impactor for CCI, Leica Microsytems) was used to perform TBI with the following parameters: 3 mm tip diameter, 18° angle, depth 0.8 mm from the dura, velocity 3 m/s, and dwell time 300 ms. Sham mice received identical anesthesia and scalp incision, but received a sham craniotomy of 3-mm diameter (in which the drill bit was used to trace a craniotomy on the skull without penetration), and the injury was not delivered. 3 days after sham or TBI procedures, a subset of mice underwent stereotaxic surgery to receive intra-thalamic injection AAV2/5-GfaABC$_1$D-GAT3-HA-mCherry (600 nL), delivered unilaterally to the VB thalamus as described above.

TBI seizure challenge assay: To determine the seizure susceptibility of mice with TBI in a high throughput manner, we assessed behavioral seizures following PTZ challenge (45 mg/kg, i.p.). PTZ dose was selected based on prior studies for C57BL6 mice in our group and others *(84)*. Mice were video-recorded for 20 minutes after PTZ, 4 and 11 weeks after TBI induction. A modified Racine scale *(85)* was used to score behavioral seizures off-line in a blinded manner. Stage 0 = normal behavior; 1 = immobility; 2 = generalized spasm, tremble, or twitch; 3 = tail extension; 4 = forelimb clonus; 5 = generalized clonic activity; 6 = bouncing or running seizures; 7 = full tonic extension; 8 = death.

Logistic regression model of TBI mouse survival following PTZ challenge

To assess the impact of astrocytic GAT-3 enhancement on mortality/survival following PTZ challenge, we used a logistic regression model consisting of trauma and GAT-3 treatment as independent variables and survival as the dependent variable (GraphPad Prism). Goodness-of-fit assessed with area under the ROC curve and the likelihood ratio test.

$$\ln(odds) = \beta_0 + \beta_1 X_1 + \beta_2 X_2, \text{ where } odds = \frac{P(Y=1)}{P(Y=0)} \text{ and Y = survival}$$

The impact of TBI and of GAT-3 on survival is represented by the β_1 and β_2 parameter estimate, respectively, of our model. The exponentiation of each parameter estimate yields an odds ratio, which represents the "multiplicative effect" that a given parameter has on survival and is reported in fig. S10.

Behavioral Assays

Behavioral tasks took place during the light cycle between 7:00 AM and 7:00 PM. Mice were transferred to the behavioral testing room at least 30 min prior to testing to acclimate to the environment and lighting, unless specified otherwise. All tasks were performed and analyzed by experimenters blinded to condition.

Open Field Activity Test: Open field activity is assessed using the Flex-Field/Open Field Photobeam Activity System (San Diego Instruments), which consists of a clear acrylic chamber (41 x 41 x 30 cm) and two sets of photobeam arrays that automatically detect horizontal and vertical movements. Mice are placed in the center of the chamber at the beginning of the test. Analysis: Ambulatory and fine movements are automatically recorded using Photobeam Activity System software (San Diego Instruments). The open field arena is divided into an outer periphery and center. Proportion of total movements in the periphery relative to the center is used to determine degree of baseline anxiety.

Elevated Plus Maze: The elevated plus maze (EPM) is elevated 30.5" above the ground, and consists of two open arms (15" x 2", length x width) and two closed arms (15" x 2" with 6.5" height walls) (Hamilton-Kinder). During the task, mice are placed at the center of the maze and allowed to explore for 10 minutes. Analysis: Total distance traveled and number of entries into closed arms are calculated based on infrared photobeam breaks, automatically detected using MotorMonitor software (Kinder Scientific). Total distance is used as a measure of general activity. Percent time spent in open arms is used as a measure of baseline anxiety.

Olfactory Habituation: In addition to transferring all mice to the testing room 1 hour prior to testing, each mouse is individually placed into a cage without bedding for 30 min prior to testing. Mice are exposed to three different odors in this order: water, vanilla, and an unfamiliar social odor. The task consists of three trials (2 min each) for each of the three odors. With an inter-odor interval of 1 min. For non-social odors, cotton tip applicators were dipped in each odor solution for 2 sec, immediately before scent presentation to avoid evaporation. Vanilla was diluted 1:100 in water. For the unfamiliar social odor, the cotton tip was used to swipe the bottom of a cage of an unfamiliar mouse of the same strain and sex several times. For each trial, the experimenter secures the cotton tip applicator to the flat wire cage top so that the tip is hanging 2 inches off the cage floor. The experimenter then moves 2 meters away from the cage to score. A new cotton tip was used for each odor. All trials are simultaneously videotaped. Analysis: The experimenter scores the odor exploration in real-time. Bouts of sniffing, as well as cumulative time spent sniffing the cotton tip, is recorded for each 2-minute trial. Sniffing is scored when the mouse is oriented towards the cotton tip with its snout 2 cm or closer to the tip. Chewing on the cotton tip is counted as sniffing, whereas

chewing on the wooden handle of the applicator or climbing the applicator is not counted as sniffing.

Hot Plate Test: During the test, mice are placed into a clear, open-ended cylinder (4" diameter) which is placed on top of a black anodized aluminum hot plate (Hot Plate Analgesia Meter, IITC Life Science). The surface of the hot plate is heated and maintained at 52°C, and cleaned with 70% EtOH between each subject. Once the mouse is placed on the hot plate, the latency to respond with either a hind paw lick, hind paw flick, or jump is measured by an experimenter. To prevent injury, the maximum latency is 30 seconds. Once the mouse responds or reaches the 30 second limit, the mouse is removed from the hot plate and returned to its home cage. Analysis: Once the mouse is placed on the hot plate, the latency to respond with either a hind paw lick, hind paw flick, or jump is measured by an experimenter.

Contextual Fear Conditioning: Mice are brought into the testing room immediately before the trial begins. The contextual fear conditioning task consists of three phases: Training, Context Test, and Generalization Test. All phases take place in a sound-isolated fear conditioning chamber (Med Associates), cleaned with 70% EtOh between trials. During the Training phase (13 min total), mice are placed in the apparatus in which the light setting is 3, fan is on, trays are sprayed with 70% Windex, and metal floor grid is exposed. Following a 5-min baseline period, mice are presented with four 2-second 0.45 mA foot shocks separated by 2-min intervals. 24 hours later, the Context Test (10 min total) takes place. Mice are placed in the same apparatus (same context) for 10 minutes, with no foot shocks delivered. The Generalization Test (10 min total) takes place 24 hours after the Context Test. The context is altered from the Training phase in the following manner: light setting is 1, fan is off, trays are sprayed with 10% Simple Green, and a solid plastic floor insert is used. Mice are placed in this apparatus for 10 minutes, with no foot shocks delivered. Analysis: Freezing during each trial is monitored by Video Freeze software (Med Associates, Inc).

Grooming: Mice were individually placed in a transparent cage for 10 minutes while being videotaped. Duration of spontaneous whisker grooming was manually quantified off-line using video footage.

10x Visium spatial transcriptomics of mouse brain after traumatic brain injury and stroke

The 10x Visium Spatial Transcriptomics pipeline was performed on three total hemisections obtained from mice 6 weeks after TBI, stroke, or a sham procedure. The brains were harvested in OCT and flash frozen on dry ice. The hemispheres were sectioned coronally to 10 μm on a cryostat and mounted on the Visium Spatial Gene Expression slide. All sections were analyzed for RNA integrity number (>8) measured by a Bioanalyzer. To visualize the section morphology and cell bodies for later spatial alignment of sequencing data, sections were methanol fixed at –20°C for 30 min and stained for hematoxylin and eosin (H&E). The sections were imaged using bright-field microscopy, then enzymatically permeabilized for 12 min, poly-A mRNA captured on each of the spots, and spatial barcodes and unique molecular identifiers (UMIs) were added to the reads. The dual-index Illumina paired-end libraries were sequenced on NovaSeq 6000, and the RNAseq reads were aligned to the mouse reference genome mm10-2020-A and images detected using SpaceRanger pipeline (v.1.3.0).

Data were visualized using 10x Loupe Browser (v.5.1.0). Raw per-spot gene expression UMIs were exported from the SpaceRanger pipeline (v.1.3.0) and aligned using barcodes (Fig. 6, fig. S8, fig. S9, and table S10). To separate out spatial regions that showed unique and most homogeneous gene expression patterns, we performed unbiased K-means clustering using 10 unique clusters for each section (fig. S8). Note that in the thalamus of the TBI section, two regions were separated out as unique clusters 7 and 4, which corresponded to the regions that showed high and low *Gfap* transcripts. After performing the differential expression of genes (DEGs) analysis of cluster 7 (fig. S8) compared to all other clusters, we determined that this region is enriched in

inflammatory markers such as *Gfap, Serpina3n, C1qa, Tyrobp*, and others (see fig. S8E for top 20 DEGs). We used this unbiased separation of thalamic clusters as a rationale for choosing two thalamic regions of interest (*Gfap*-High and *Gfap*-Low) (Fig. 6). We chose two cortical regions of interest which were proximal and distal to the injury site (fig. S9).

For investigations of individual genes such as *Gfap* and *Slc6a11*, we performed Kolmogorov-Smirnov tests and adjusted α=0.025 to correct for multiple (two) comparisons made within each sample: *Gfap*-High vs. *Gfap*-Low thalamus, and *Gfap*-High vs. *Gfap*-Low cortex. To assess the relationship between *Gfap* and *Slc6a11*, a simple linear regression was performed separately for cortical and thalamic data. Statistical analyses were performed within-section between *Gfap*-High and *Gfap*-Low regions in the thalamus, and between proximal and distal regions in the cortex.

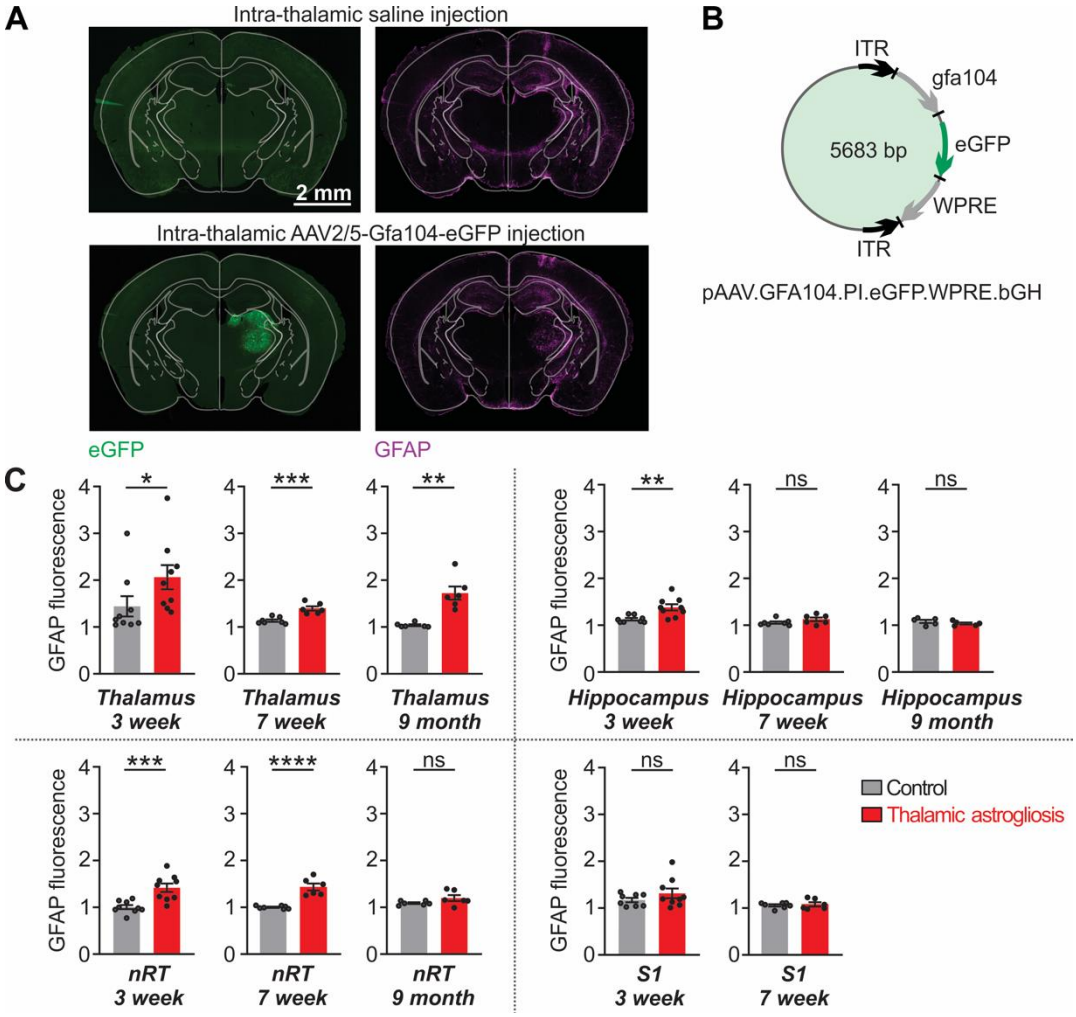

Fig. S1. Persistent increase of GFAP protein in thalamus following viral-mediated astrogliosis. **(A)** Immunohistochemical labeling of enhanced green fluorescent protein (eGFP) and glial fibrillary acidic protein (GFAP) following unilateral injection of either saline (top) or AAV2/5-Gfa104-eGFP (bottom) into the ventrobasal (VB) thalamus. Note that the representative images of the AAV2/5-Gfa104-eGFP injection are the same images presented in Fig. 1D, and are included here for visual comparison. **(B)** Schematic of the pAAV.GFA104.PI.eGFP.WPRE.bGH plasmid used to produce the AAV2/5-Gfa104-eGFP construct. Adapted from *(35)*, Fig. 1H. Four solid black lines indicate multiple cloning sites. Sequence map is available through Addgene (Plasmid #100896). Note that when the *Gfa104* promoter is used with the AAV2/5 pseudotype, the viral construct leads to >99% astrocyte-specific expression *(35)*. **(C)** GFAP fluorescence in thalamus (including ventroposterior medial, ventroposterior lateral, ventrolateral, posterior medial, dorsal lateral geniculate, and lateral posterior nuclei), reticular thalamic nucleus (nRT), hippocampus, and primary somatosensory cortex (S1). Fluorescence ratio between regions ipsilateral and contralateral to injection site, obtained three weeks, seven weeks, and nine months after induction of thalamic astrogliosis. Data from thalamus (three week timepoint) are the same data presented in Fig. 1D, and included here for visual comparison. **3 weeks:** n=8-9 mice per group (data averaged from 3 sections/mouse). Mann-Whitney U-test for thalamus (**P*=0.018), nRT (***P*=0.001), hippocampus (***P*=0.0016), and S1 (ns, *P*=0.54). ns: not significant. **7 weeks:** n=6-7 mice per group. Mann-Whitney U-test for thalamus (***P*=0.0012), nRT (***P*=0.0012), hippocampus (ns, *P*=0.295), and S1 (ns, *P*>0.99). **9 months:** n=5-6 mice per group. Mann-Whitney U-test for thalamus (***P*=0.002), nRT (ns, *P*=0.18), hippocampus (ns, *P*=0.42). **Related to Figure 1.**

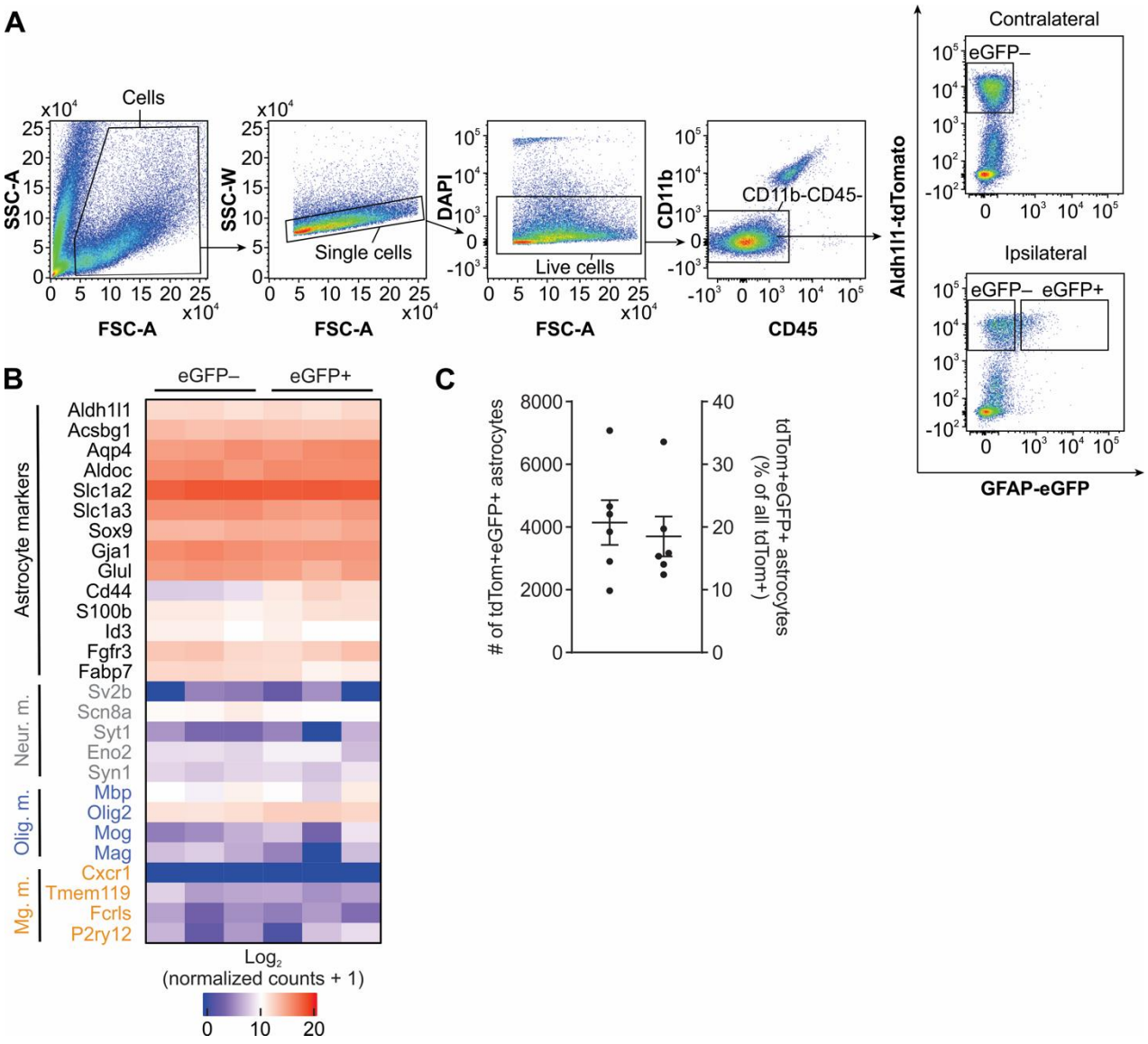

Fig. S2. Molecular characterization of FACS-isolated thalamic reactive astrocytes. (A) Fluorescence activated cell sorting (FACS) gating strategy for samples collected for RNA sequencing, obtained from the thalamus ipsilateral and contralateral to intra-thalamic transduction of astrocytes in pan-astrocytic reporter Aldh1l1-tdTomato mice. Gates indicate sorting strategy to obtain ipsilateral virally transduced "reactive" astrocytes (tdTomato^{+}eGFP^{+}), and contralateral "healthy" astrocytes (tdTomato^{+}eGFP$^{—}$). Astrocytes were gated as DAPI$^{—}$, CD11b$^{—}$ and CD45$^{—}$ followed by Aldh1l1-tdTomato^{+}, GFAP-eGFP$^{—}$ for the contralateral side and Aldh1l1-tdTomato^{+}, GFAP-eGFP$^{—}$ (eGFP–) and Aldh1l1-tdTomato^{+}, GFAP-eGFP^{+} (eGFP+) for the ipsilateral side. FSC-A: forward scatter area; SSC-A: side scatter area; SSC-W: side scatter height. Isolated astrocytes were subsequently used for RNA sequencing (RNA-Seq). **(B)** Heat map of cell-type specific markers, demonstrating the specificity of our FACS approach to isolate astrocytes that showed high expression of astrocytic markers such as *S100b* (indicated in black), and low expression of neuronal markers such as *Syt1* (grey), oligodendrocyte markers such as *Mbp* (blue), and microglial markers such as *Cxcr1* (orange). Color gradient indicates log2 of the normalized counts (+1) for each gene from the RNA sequencing data of contralateral eGFP– and ipsilateral reactive eGFP+ astrocytes. **(C)** Number (left y-axis) and percentage (right y-axis) of FACS-isolated tdTom^{pos}eGFP^{pos} astrocytes in ipsilateral thalami. 18.5 $\pm$ 0.03% of tdT+ astrocytes were eGFP+. n=6 samples. **Related to Figure 1.**

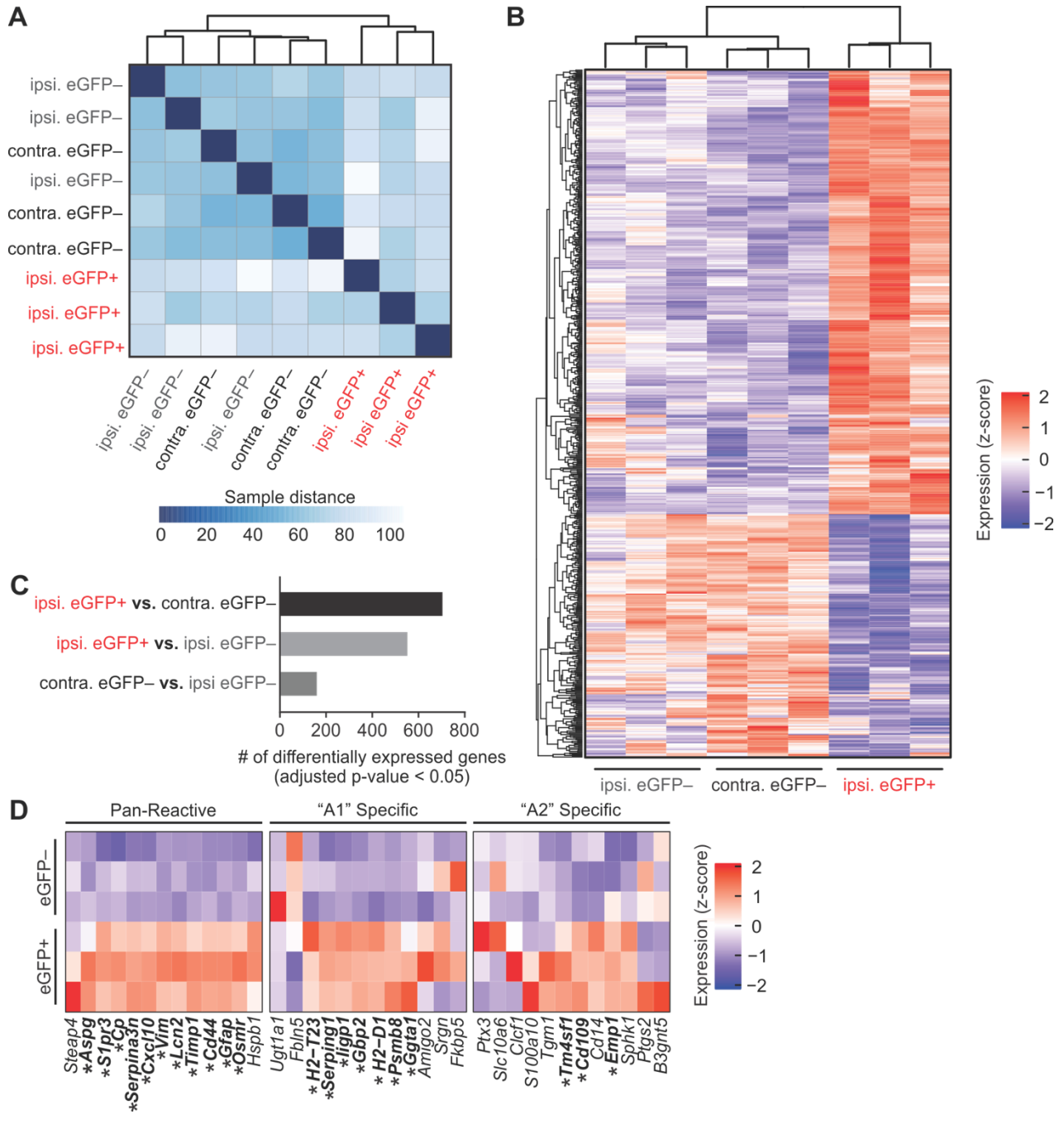

Fig. S3. Transcriptomic comparison of eGFP-positive and eGFP-negative thalamic astrocytes. **(A)** Hierarchical clustering of sample distance, a measure of sample-to-sample similarity, reveals clustering of ipsilateral eGFP-positive (eGFP+) astrocyte samples away from ipsilateral eGFP-negative and contralateral eGFP-negative (eGFP–) astrocyte samples. **(B)** Heat map of differentially expressed genes (DEGs) in eGFP+ versus eGFP– thalamic astrocytes (adjusted *P* value < 0.05). Dendograms indicate hierarchical clustering of DEGs. Heat map shows z-scored expression of DEGs in contralateral eGFP–, ipsilateral eGFP–, and ipsilateral eGFP+ astrocytes. Note that the ipsilateral eGFP+ and contralateral eGFP– astrocyte samples are the same as those shown in Figure 1H. **(C)**

Number of differentially expressed genes (adjusted P value < 0.05). **(D)** Heat map showing expression of "pan-reactive", lipopolysaccharide-induced ("A1")- and middle cerebral artery occlusion-induced ("A2")- reactive astrocyte genes (as reported in *(31)*) in contralateral thalamic eGFP-negative and ipsilateral thalamic reactive eGFP-positive astrocytes. * indicates genes which were significantly upregulated in ipsilateral thalamic reactive eGFP-positive astrocytes. 11 "pan-reactive" genes which were significantly upregulated are highlighted in Figure 1H. Adjusted *P<0.05. Color gradient indicates z-scored relative expression. **Related to Figure 1.**

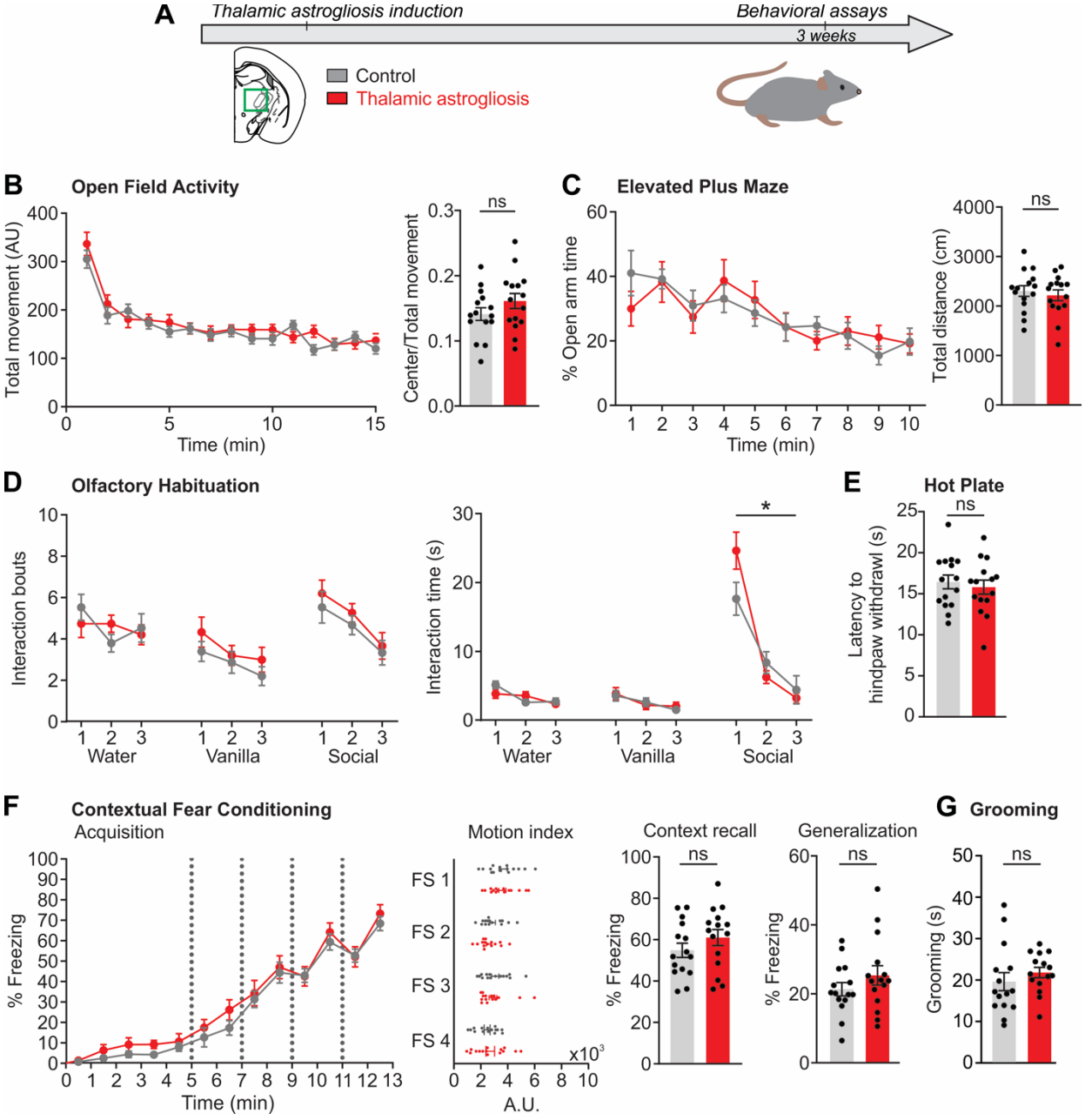

Fig. S4. Behavioral repertoire in mice with thalamic astrogliosis. (A) Schematic of experimental timeline. Three to four weeks after viral transduction of thalamic astrocytes, mice underwent behavioral testing to assess spontaneous locomotion, anxiety, olfactory habituation, aversion, and contextual learning and memory performance. n=15 mice/group. **(B)** Open field activity. Left: total movement throughout a 15-minute session. Two-way repeated measures ANOVA, $F(14, 392)$, Interaction P=0.19. Shapiro-Wilk normality test, P>0.05. Right: ratio of movement in the center vs. total arena. Mann-Whitney U test, P=0.29. ns: not significant. **(C)** Elevated plus maze. Left: percentage of time exploring open arm throughout a 10-minute session. Two-way repeated measures ANOVA with Geisser-Greenhouse correction, $F(9, 252)$, Interaction P=0.73. Shapiro-Wilk normality test, P>0.05. Right: total distance traveled. Mann-Whitney U test, P=0.74. **(D)** Olfactory habituation test. Mice were presented with three trials each of three distinct odors: water, vanilla, and an unfamiliar social odor.. Two-way repeated measures ANOVA with Geisser-Greenhouse correction, $F(2,56)$. Interaction Bouts: Water (P=0.27), Vanilla (P=0.82), Social (P=0.96). Interaction Time: Water (P=0.14), Vanilla (P=0.78), Social (*P=0.03; no significant multiple

comparisons, with Sidak's correction for multiple comparisons). Shapiro-Wilk normality test, $P>0.05$. **(E)** Hot plate test. Latency to withdraw left hindpaw (contralateral to thalamic astrogliosis) in response to an aversive stimulus. Mann-Whitney U test, $P=0.83$. **(F)** Contextual fear conditioning. *Acquisition:* percentage of time spent freezing during the acquisition phase. Dashed vertical lines indicate time of foot shocks.Two-way repeated measures ANOVA with Geisser-Greenhouse correction, $F(12, 336)$, Interaction $P=0.96$. Shapiro-Wilk normality test, $P>0.05$. *Motion Index*: movement in response to foot shocks (FS). Multiple Mann-Whitney U test design with Holm-Sidak correction. FS 1 ($P>0.99$), FS 2 ($P=0.82$), FS 3 ($P=0.95$), FS 4 ($P=0.95$). *Context Recall*: percentage of time spent freezing during the recall phase. Mann-Whitney U test, $P=0.27$. *Generalization*: percentage of time spent freezing during the generalization phase. Mann-Whitney U test, $P=0.26$. **(G)** Grooming. Total time spent grooming whiskers during a 10-minute session. Mann-Whitney U-test, $P=0.15$. **Related to Figure 1.**

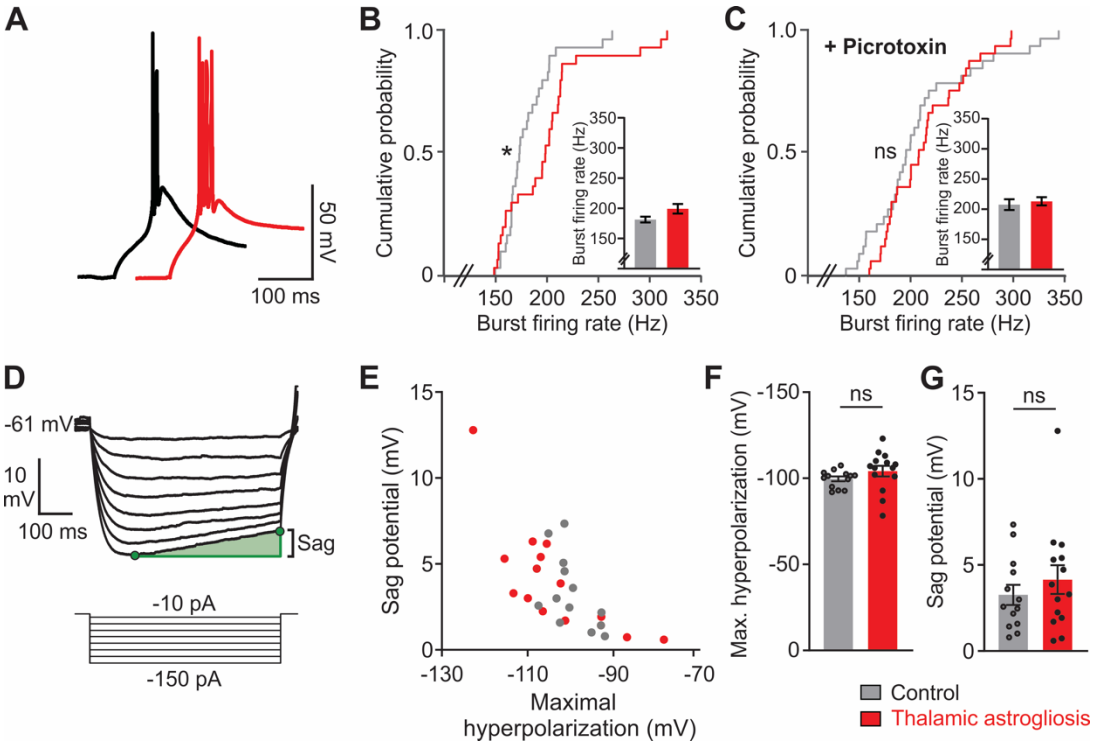

Fig. S5. Properties of hyperpolarization-induced rebound bursting and depolarizing sag potential in thalamocortical neurons. (A) Overlay of the hyperpolarization-induced rebound burst firing from two representative thalamocortical neurons in response to the same current injection (-130 pA). **(B)** Cumulative probability distribution of the action potential firing rate during the first hyperpolarization-induced rebound burst response. Population data consists of the firing rate obtained from the three most hyperpolarized sweeps for each cell to ensure equal representation. Inset shows bar plot mean ± SEM. Kolmogorov-Smirnov test, **P*=0.026. Control: 3 sweeps/neuron, n=10 neurons; Thalamic astrogliosis: 3 sweeps/neuron, n=10 neurons. **(C)** Same as in (B), but in presence of Picrotoxin. Kolmogorov-Smirnov test, *P*=0.62. ns: not significant. Control: 3 sweeps/neuron, n=11 neurons; Thalamic astrogliosis: 3 sweeps/neuron, n=11 neurons. **(D)** Hyperpolarization-induced 'sag' depolarization was measured in response to hyperpolarizing current steps. The amplitude of the sag depolarization (green shaded region) was calculated as the difference between the maximal hyperpolarized membrane potential and the membrane potential at the end of the current injection. All cells were recorded at resting membrane potential. **(E)** Amplitude of the sag potential as a function of the maximal hyperpolarized potential in response to a -150 pA intracellular current injection. **(F)** Maximal hyperpolarization. Mann-Whitney U test, *P*=0.053. Control: n=13 neurons; Thalamic astrogliosis: n=14 neurons. **(G)** Amplitude of the depolarizing sag potential. Mann-Whitney U test, *P*=0.52. **Related to Figure 3.**

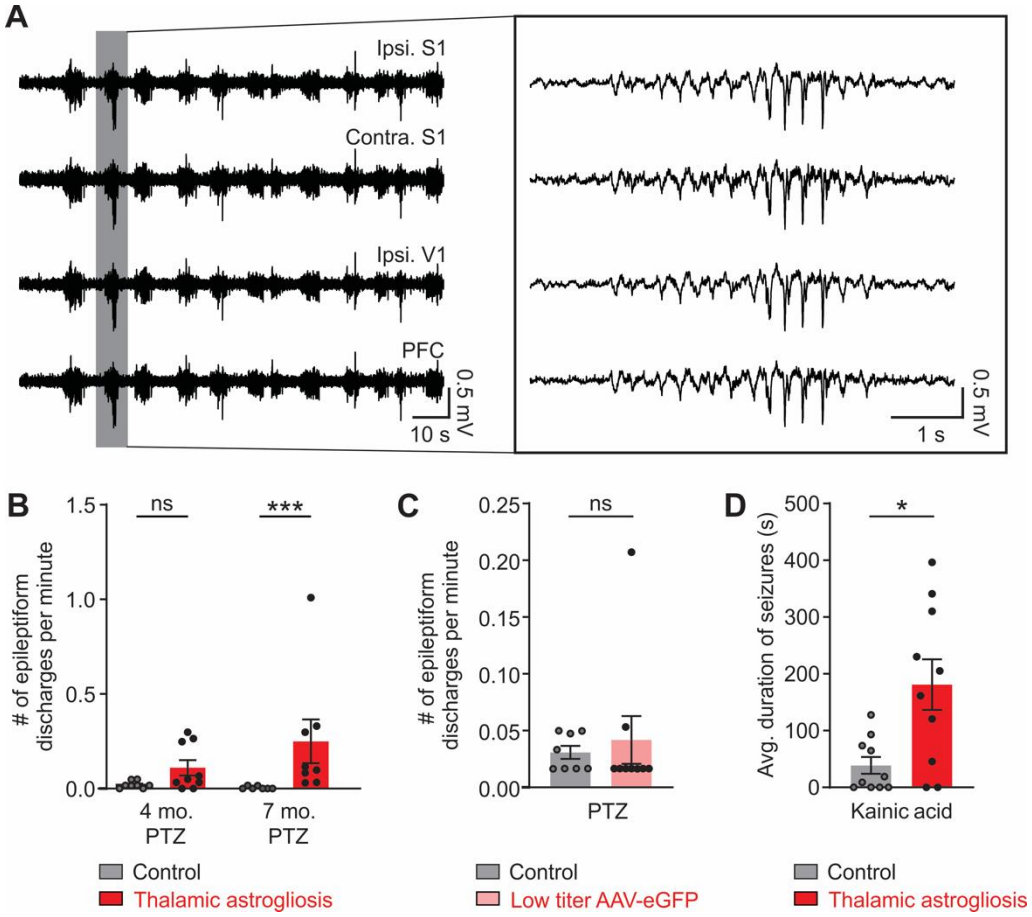

Fig. S6. Characterization of enhanced seizure risk. (A) Representative ECoG traces in the PTZ challenge experiment from the mouse with thalamic astrogliosis shown in Fig. 3, B and C. Here, we include ECoG traces simultaneously obtained from primary somatosensory cortex S1 ipsilateral and contralateral to site of thalamic astrogliosis, as well as ipsilateral primary visual cortex and prefrontal cortex. **(B)** Quantification of ipsilateral S1 cortical epileptiform discharges induced by PTZ (5 mg/kg), 4 and 7 months after viral-mediated astrogliosis. 4 months: Mann-Whitney U test, *P*=0.10; Control: n=8 mice; Thalamic astrogliosis: n=9 mice. 7 months: Mann-Whitney U test, ****P*=0.0003; Control: n=7 mice; Thalamic astrogliosis: n=8 mice. P-values are not adjusted for multiple comparisons or within-subject comparisons. ns: not significant. **(C)** Quantification of ipsilateral S1 cortical epileptiform discharges induced by a low titer injection of AAV2/5-Gfa104-eGFP (see Methods). Mann-Whitney U test, *P*=0.98. Control: n=8 mice; Thalamic astrogliosis: n=9 mice. **(D)** Average duration of seizures induced by Kainic Acid (10 mg/kg). Mann-Whitney U test, **P*=0.025, n=10 mice/group. **Related to Figure 4.**

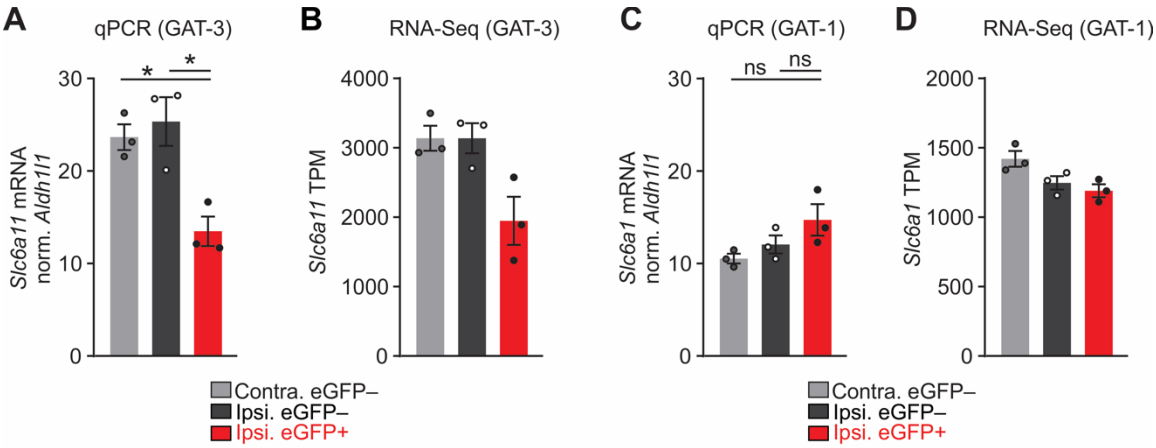

Fig. S7. GAT-3, but not GAT-1, is reduced at the transcript level in eGFP-positive thalamic reactive astrocytes. (A) *Slc6a11* expression (encoding GAT-3), normalized to *Aldh1l1* expression in FACS-isolated astrocytes. Transcript expression obtained by quantitative PCR (qPCR). FACS was performed to isolate astrocytes from the thalamus, ipsilateral and contralateral to stereotaxic injection of AAV2/5-Gfa104-eGFP in adult Aldh1l1-tdTomato reporter mice. Sorting strategy to obtain astrocytes detailed in Fig. S2. Note that data in (A) is presented in Fig. 5C and included here for visual comparison. One-way ANOVA: $F(2,6)=10.89$, $^*P=0.01$. Shapiro-Wilk normality test, $P>0.05$. Tukey's multiple comparisons: contra. eGFP– vs. ipsi eGFP– (ns, $P=0.816$), contra.eGFP– vs. ipsi eGFP+ ($^*P=0.024$), ipsi eGFP– vs. ipsi eGFP+ ($^*P=0.012$), n=3 mice. **(B)** Normalized gene expression of *Slc6a11*, expressed as Transcripts Per Million (TPM), obtained from our RNA sequencing (RNA-seq) experiment in FACS-isolated astrocytes as described in (A). **(C)** Same as in (A), but for *Slc6a1* (encoding GAT-1). One-way ANOVA, $P=0.11$, Shapiro-Wilk normality test, $P>0.05$. n=3 mice. ns: not significant. **(D)** Same as in (B), but for *Slc6a1*. **Related to Figure 5.**

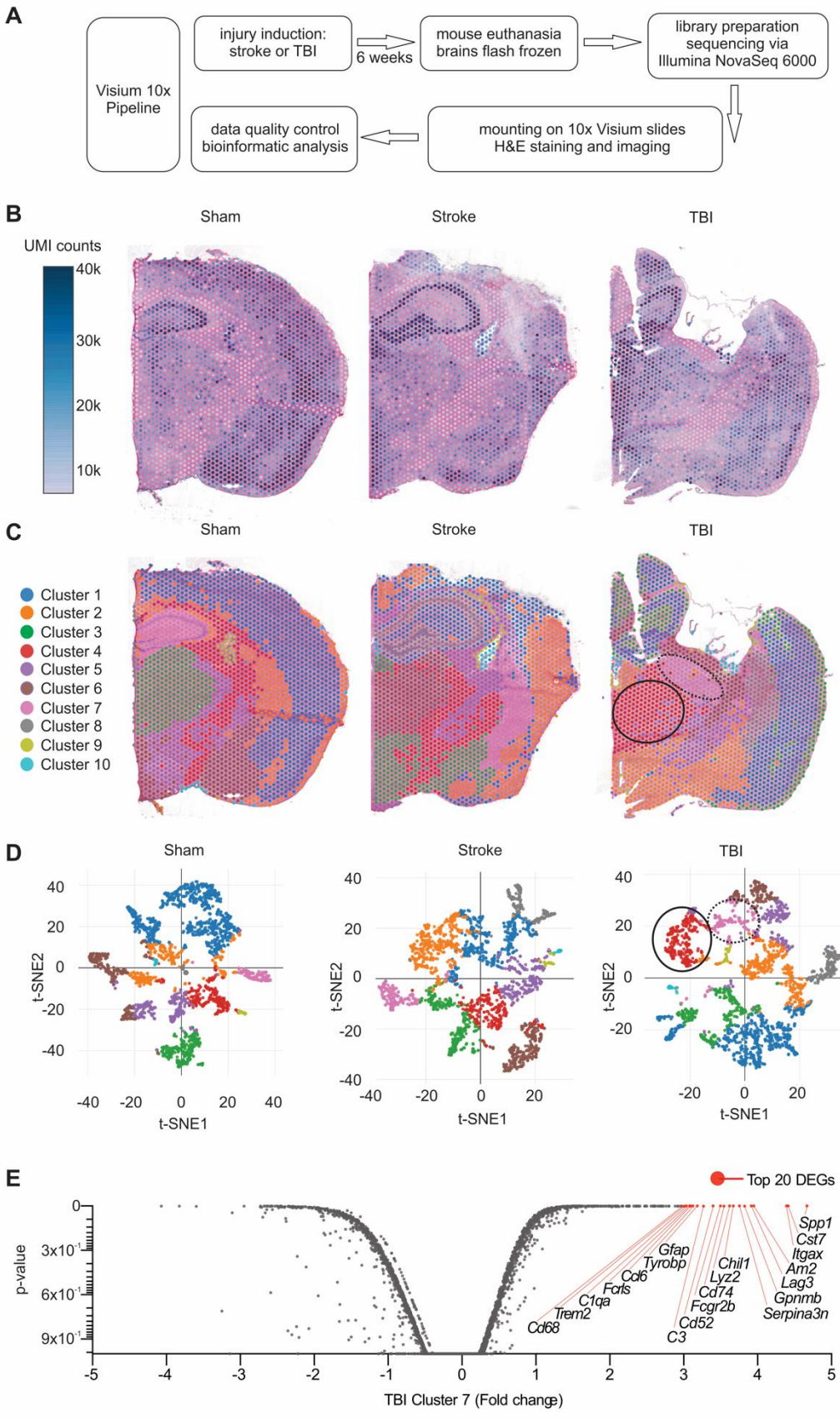
A
Visium 10x Pipeline
injury induction: stroke or TBI
6 weeks
mouse euthanasia brains flash frozen
library preparation sequencing via Illumina NovaSeq 6000
mounting on 10x Visium slides H&E staining and imaging
data quality control bioinformatic analysis
B
Sham
Stroke
TBI
UMI counts
40k
30k
20k
10k
C
Sham
Stroke
TBI
Cluster 1
Cluster 2
Cluster 3
Cluster 4
Cluster 5
Cluster 6
Cluster 7
Cluster 8
Cluster 9
Cluster 10
D
Sham
Stroke
TBI
t-SNE1
t-SNE2
E
Top 20 DEGs
p-value
TBI Cluster 7 (Fold change)
Spp1
Cst7
Itgax
Am2
Lag3
Gpnmb
Serpina3n
Chil1
Lyz2
Cd74
Fcgr2b
Cd52
C3
Gfap
Tyrobp
Ccl6
Fcrls
C1qa
Trem2
Cd68

Fig. S8. Spatial transcriptomic analysis of mouse brains after injury. (A) Schematic of experimental approach for spatial transcriptomics of mice six weeks after stroke or TBI injury. **(B)** Data quality control (QC): tissue plots with spots colored by unique molecular identifier (UMI) count. See Table S10 for more data QC measures. **(C)** Separation of spatial regions into 10 clusters using an unbiased k-means clustering algorithm. Each cluster is marked with a unique color. In the TBI section (right), two thalamic regions separated out as unique clusters 7 and 4, corresponding to *Gfap*-High and *Gfap*-Low thalamic regions analyzed in Fig. 7. **(D)** t-SNE projection of spots in each cluster. Cluster 7 from **(C)** is outlined in dotted line, Cluster 4 from **(C)** is outlined in solid line. **(E)** Differentially expressed genes (DEGs) in TBI *Gfap*-High thalamus (Cluster 7). Top 20 significant DEGs (note, all of them are upregulated) are marked in red. **Related to Figure 7.**

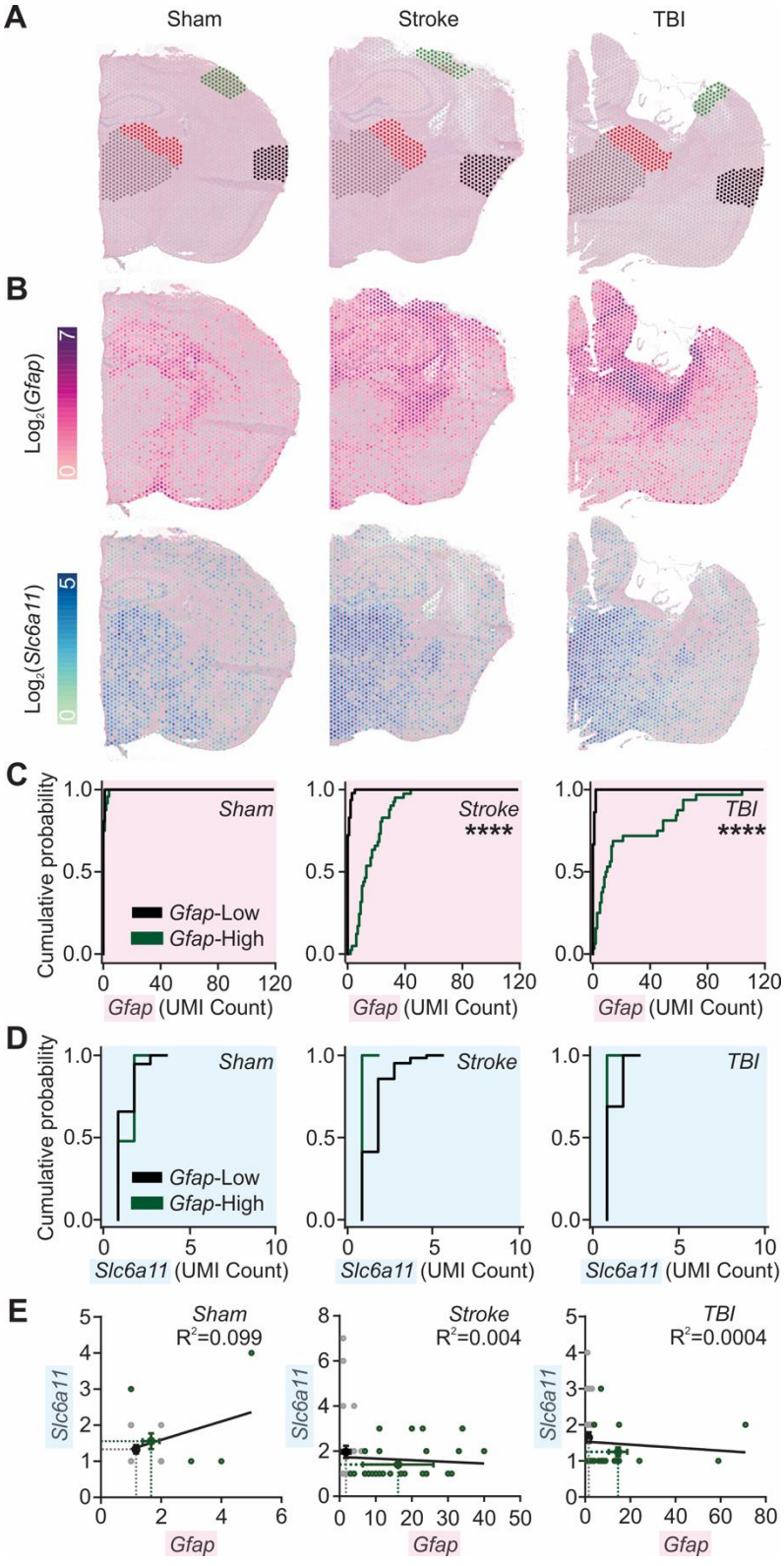
A
Sham
Stroke
TBI
B
Log2(Gfap)
7
0
Log2(Slc6a11)
5
0
C
Cumulative probability
Sham
Stroke
****
TBI
****
Gfap-Low
Gfap-High
Gfap (UMI Count)
D
Slc6a11 (UMI Count)
E
Sham
R2=0.099
Stroke
R2=0.004
TBI
R2=0.0004
Slc6a11
Gfap

Fig. S9. Lack of correlation of cortical *Gfap* and *Slc6a11* transcript expression in mouse models of cortical injury. (A) Hemi-brain sections from mice after sham, stroke, and TBI procedures six weeks after surgery overlaid with regions analyzed with 10x Visium spatial transcriptomics. Black and green spots indicate cortical regions with high and low *Gfap* expression in cortical injury. Red and grey spots indicate thalamic regions with high and low *Gfap* expression in cortical injury, as indicated in Fig. 7. **(B)** Cortical expression of *Gfap* and *Slc6a11* transcripts. Color map indicates log2 of the detected counts of the gene's unique molecular identifier (UMI). **(C, D)** Cumulative probability distribution of *Gfap* (C) or *Slc6a11* (D) expression per spot in regions indicated in (A). Kolmogorov-Smirnov test, ****P<0.0001. All spots containing non-zero UMI counts were included. Number of spots from low- and high-*Gfap* regions (or, distal and proximal cortex), respectively, in (C): sham (n=26 & 24); stroke (n=47 & 41); TBI (n=51 & 32); in (D): sham (n=40 & 51); stroke (n=64 & 26); TBI (n=62 & 13). Adjusted α=0.025 for multiple comparisons. **(E)** Relationship between *Gfap* and *Slc6a11* expression. Circles represent UMI counts per spot in low- (black) and high-*Gfap* (green) areas; black and green crosses, and corresponding dotted lines, mark mean$\pm$SEM for low- and high-*Gfap* areas respectively. Black lines plot the best-fit slopes and intercepts from a simple linear regression. Number of spots: sham (n = 36), stroke (n = 62), and TBI (n = 57). **Related to Figure 7.**

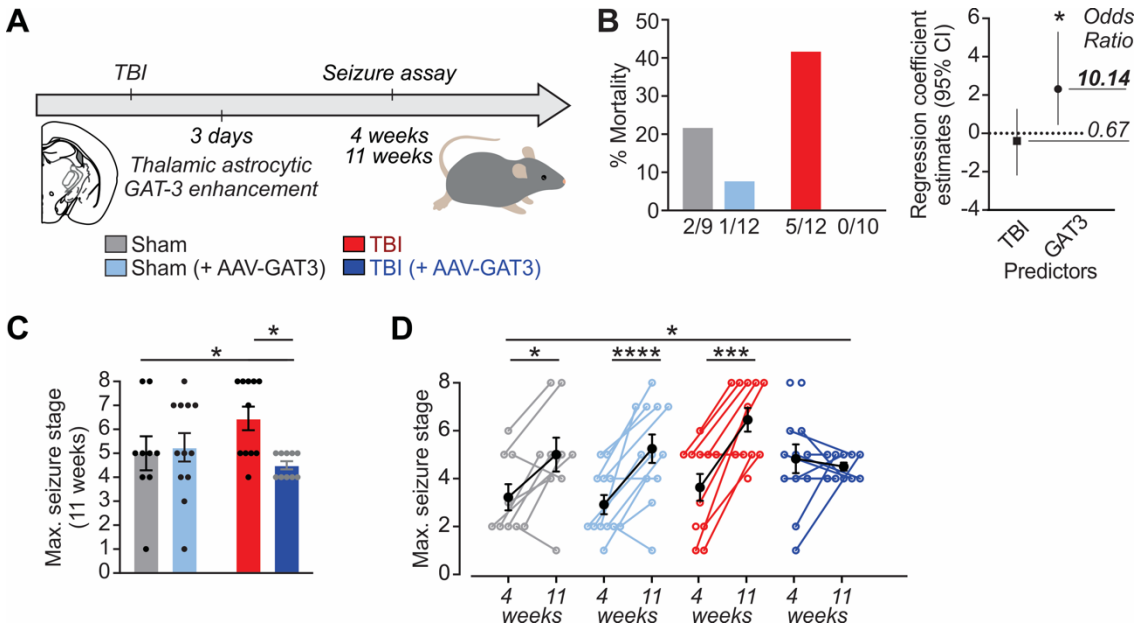

Fig. S10. Enhancing GAT-3 in a mouse model of TBI reduces PTZ-induced seizure severity and mortality. (A) Schematic of experimental design. In a controlled cortical impact model of traumatic brain injury, a metal piston (3 mm diameter) is used to deliver an impact at a depth of 0.8 mm to the right somatosensory cortex. Three days following injury or sham procedure, increased GAT-3 expression in thalamic astrocytes was achieved by transducing thalamic astrocytes with AAV2/5-GfaABC1D-GAT3-mCherry *(54)* in a subset of mice. We assessed seizure susceptibility at two timepoints (four and eleven weeks post-injury) reported to reflect the "subacute" and "chronic" stages of TBI-induced epileptogenesis and hyperexcitability *(86, 87)*. **(B)** *Left:* probability of death following PTZ-induced seizures. Numbers below x-axis indicate the number of deaths as a fraction of the total number of mice in each group. . *Right:* estimates of regression coefficients (representing log odds ratio of survival) obtained from a logistic regression model (81.4% classification performance; area under the ROC = 0.757, **P*=0.025). The impact of each predictor on survival is obtained from the exponentiation of the parameter estimate into an odds ratio (**P*=0.04). Error bars indicate 95% confidence intervals. **(C)** Seizure severity assessed 20 minutes following PTZ (45 mg/kg, i.p.), eleven weeks after injury. Behavioral characterization of seizure stage is scored according to the Racine scale, with stage 8 = death. Sham: n=9 mice; Sham + GAT-3: n=12 mice; TBI: n=11 mice; TBI + GAT-3: n=10 mice. A two-way ANOVA was performed to account for two factors (trauma and treatment): Interaction ($F(1,38)=4.3$, **P*=0.045). Post-hoc Sidak's multiple comparisons: TBI vs. TBI+GAT-3 (adjusted **P*=0.026). Shapiro-Wilk normality test: Sham (*P*>0.05), Sham+GAT-3 (*P*>0.05), TBI (***P*=0.0044), TBI+GAT-3 (****P*=0.0003). α=0.05. An alternative non-parametric analysis (which does not account for both factors, trauma and treatment) was performed as follows: two pairwise comparisons using the non-parametric Mann-Whitney U test, and adjustment of α=0.025 for multiple comparisons. Sham vs. Sham+GAT-3 (*P*=0.88), TBI vs. TBI+GAT-3 (**P*=0.016). Either analysis (two-way ANOVA or multiple Mann-Whitney U tests) supports our conclusion that GAT-3 treatment resulted in reduced seizure severity following TBI. **(D)** Comparison of seizure severity induced by PTZ at 4 and 11 weeks. Mixed-effects model: Interaction ($F(3,37)=3.85$, **P*=0.017). Post-hoc comparisons of 4 vs. 11 weeks: Sham (**P*=0.021), Sham+GAT-3 (*****P*<0.0001), TBI (****P*=0.0003), TBI+GAT-3 (ns; *P*=0.97). **Related to Figure 7.**

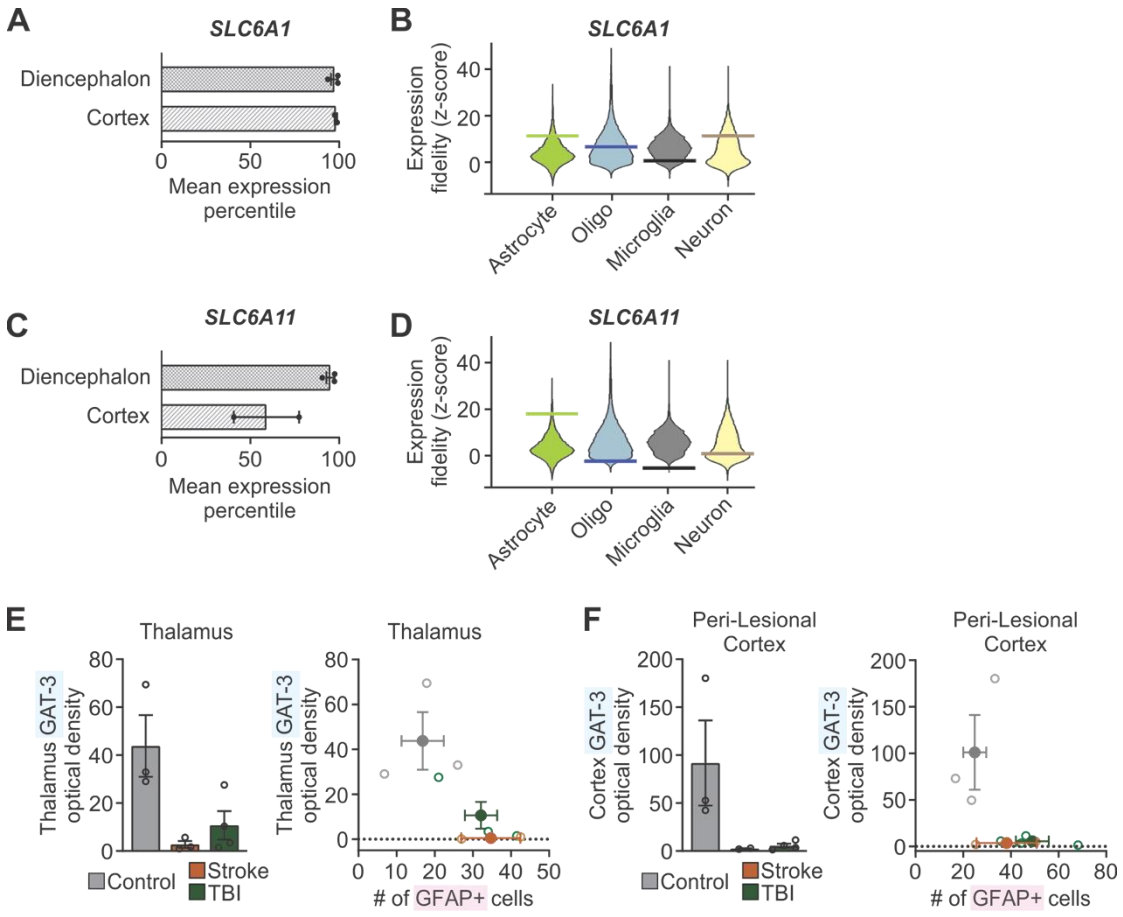

Fig. S11. *SLC6A1 and SLC6A11 gene* expression, and GAT-3 immunofluorescence in adult brain tissue. (A) Mean expression percentile of *SLC6A1* gene expression relative to all genes in neurotypical adult human diencephalon and parietal cortex. Data obtained from *(55)*. **(B)** Expression fidelity of *SLC6A1*, obtained from cell-type specific transcriptomic profiling in the adult human diencephalon compared to transcriptional signatures of major brain cell types, relative to all human genes detected in the database compiled by *(55)*. Higher fidelity indicates higher correlation of *SLC6A1* to cell type. Horizontal bar indicates Z-score for *SLC6A1* relative to that cell type, violin plot indicates Z-score distribution for all genes detected in that cell type. **(C)** Same as in (A), but for *SLC6A11* (presented in Fig. 8, shown here for clarity). **(D)** Same as in (B), but for *SLC6A11* (presented in Fig. 8, shown here for clarity). **(E, F)** Quantification of GAT-3 and GFAP immunofluorescence obtained from post-mortem tissue from human subjects with a history of ischemic stroke or TBI, and age-matched control subjects (data shown in Fig. 8C, D). *Left*: Optical density of thalamic (E) and cortical (F) GAT-3 immunofluorescence. *Right*: relationship between number of GFAP+ cells and GAT-3 immunofluorescence, averaged across images per subject (open circles). Closed circles indicate mean+SEM. *(E, Left)* Control: n=3 subjects (10 images); Stroke: n=3 subjects (8 images); TBI: n=4 subjects (16 images). *(E, Right)* Control: n=3 subjects (10 images); Stroke: n=2 subjects (4 images); TBI: n=4 subjects (16 images). *(F, left):* Control: n=3 subjects (8 images); Stroke: n=2 subjects (6 images); TBI: n=4 subjects (11 images). *(F, Right):* Control: n=3 subjects (6 images); Stroke: n=2 subjects (3 images); TBI: n=4 subjects (11 images). **Related to Figure 8.**

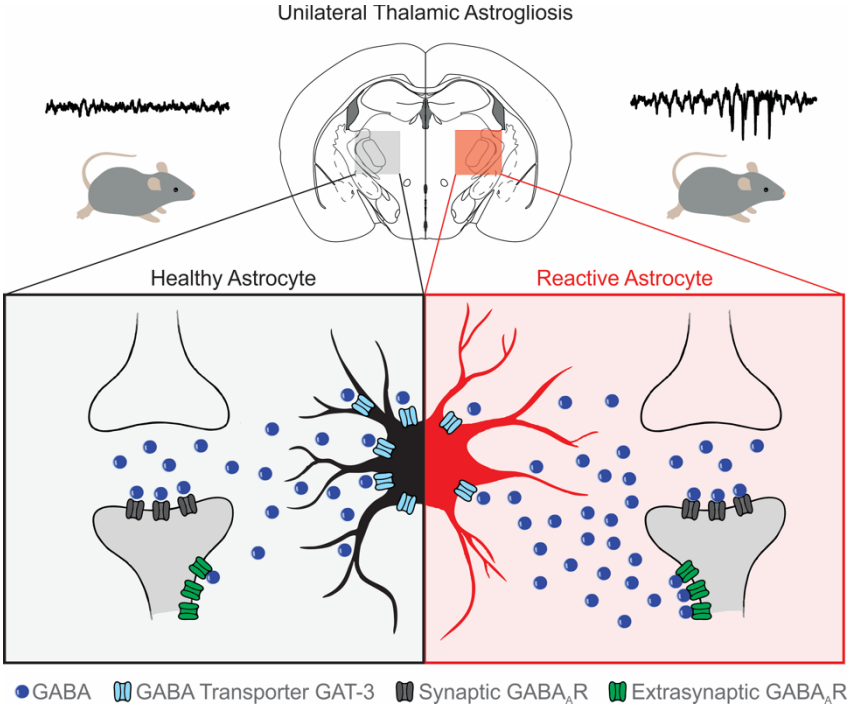

Fig. S12. Graphical summary: Neuroinflammation uses GAT-3 as a substrate to trigger cellular hyperexcitability and seizure risk. Unilateral induction of thalamic astrogliosis in adult wildtype mice (Fig. 1) is sufficient to enhance seizure risk and drive abnormal thalamocortical rhythmogenesis *in vivo* (Fig. 2, 3, 4, 6). **Left:** schematic of an unperturbed, "healthy" astrocyte (black) in the thalamus with normal expression of the GABA transporter GAT-3 (light blue), responsible for uptake of GABA (blue). **Right:** schematic of a reactive astrocyte (red) in the thalamus with decreased expression of GAT-3, which is responsible for GABA uptake. The increased availability of GABA in the extrasynaptic regions of the post-synaptic neuron (gray) explains the three-fold increase in the tonic GABA current or I_{TONIC}—mediated by extrasynaptic $GABA_A$ receptors (green)—observed in thalamocortical neurons from *ex vivo* slices affected by astrogliosis (Fig. 3E). Note that the frequency and kinetics of inhibitory postsynaptic currents—mediated by synaptic $GABA_A$ receptors (dark gray)—were unaltered (Fig. 3F, table S7 and S8). Blocking increased I_{TONIC} by conditional deletion of the extrasynaptic $GABA_AR$ (Fig. 4, H to J) or by enhancing astrocytic GAT-3 (Fig. 5, D to F) prevented astrogliosis-induced seizure risk. **Related to Fig. 1 to 8.**

Table S1.

Case	Pathology	Age	Gender	Cause of Injury	Lesion	Time after Lesion	Cause of Death
1	Control	63	F	-	-	-	Myocardial infarction
2	Control	65	M	-	-	-	Myocardial infarction
3	Control	49	M	-	-	-	Myocardial infarction
4	TBI	79	M	Fall – head injury	TC	8 d	Bronchopneumonia
5	TBI + Epi.	35	M	Horse kick – head injury	FC +TC	6 m	Myocardial infarction
6	TBI + Epi.	52	M	Car accident – head injury	FC + TC	38 y	Bronchopneumonia
7	TBI + Epi.	80	M	Grenade – head injury	FC + TC	54 y	Rupture of an abdominal aneurysm
8	IS	45	M	Infarct arteria cerebri media	FC + PC	1 d	Infarct arteria cerebri media
9	IS + Epi.	67	M	Infarct arteria cerebri media	MCA	19 y	Infarct arteria cerebri media
10	Epi. + IS	69	M	Infarct arteria cerebri media	MCA	3 y	Infarct arteria cerebri media

Case	Pathology	Age Onset Epilepsy	Seizures per Month	Seizure Type	Anti-epileptic Drugs	Post-mortem Delay (hours)
1	Control	-	-	-	-	8
2	Control	-	-	-	-	10
3	Control	-	-	-	-	9
4	TBI	-	-	-	-	11
5	TBI + Epi.	35	5	FIA	CBZ	10
6	TBI + Epi.	15	2-5	FIA	LEV, OXC	9
7	TBI + Epi.	26	2-5	FIA	CBZ, LEV	9
8	IS	45	-	-	-	10
9	IS + Epi.	21	5	FIA	CBZ, LMT	11
10	Epi. + IS	46	3	FIA	LEV, LMT	12

Table S1. Clinical characteristics of human post-mortem brain samples.
Related to Fig. 1 and 7.
d= day(s), epi= epilepsy, IS= ischemic stroke, TBI= traumatic brain injury, MCA= middle cerebral artery, FC= frontal cortex, PC= parietal cortex, TC= temporal cortex, d= days, m= months, y= years. FBTCS, focal to bilateral tonic-clonic; FIA, focal impaired awareness; LEV, Levetiracetam; LMT, Lamotrigine; OXC, Oxcarbazepine; PB, phenobarbital; CBZ, carbamazepine.

Table S2.

GFAP Immunoreactivity

	Age	Time after TBI/Stroke	Cortex Lesional	Cortex Perilesional	Thalamus
Control	63	-		1	2
	65	-		1	1
	49	-		2	1
Median (min-max)				**1 (1-2)**	**1 (1-2)**
TBI	79	8 d	3	2	2
	35	6 m	3	3	3
	52	38 y	3	3	2
	80	54 y	2	1	1
Median (min-max)			**3 (2-3)**	**2.5 (1-3)**	**2 (1-3)**
Stroke	45	1 d	3	3	3
	69	3 y	3	3	2
	67	19 y	3	3	3
Median (min-max)			**3**	**3**	**3 (2-3)**

GAT-3 Immunoreactivity

	Age	Time after TBI/Stroke	Cortex Lesional	Cortex Perilesional	Thalamus
Control	63	-		2	3
	65	-		3	3
	49	-		2	3
Median (min-max)				**2 (2-3)**	**3**
TBI	79	8 d	1	2	3
	35	6 m	1	3	3
	52	38 y	1	2	2
	80	54 y	1	2	2
Median (min-max)			**1**	**2 (2-3)**	**2.5 (2-3)**
Stroke	45	1 d	1	3	1
	69	3 y	2	2	2
	67	19 y	1	2	2
Median (min-max)			**1 (1-2)**	**2 (2-3)**	**2 (1-2)**

Table S2. Semi-quantitative analysis of GFAP immunofluorescence and GAT-3 immunoreactivity in human brain tissue. Related to Fig. 1 and Fig. 8

Immunoreactivity of glial fibrillary acidic protein (GFAP) and the extent of astrocyte reactivity was scored semi-quantitatively in the lesional cortex, perilesional cortex, and the thalamus, as follows: 1=sparsely present with resting morphology; 2=moderately present with either resting or partially reactive morphology; 3=highly present with reactive morphology. d=days; m=months; y=years. TBI=traumatic brain injury. Immunoreactivity of the GABA transporter GAT-3 was scored semi-quantitatively in the lesional cortex, perilesional cortex, and the thalamus, as follows: 0=absent, 1=sparse, 2=moderate, 3=dense staining.

Table S3.

	V_{REST} (mV)	I_{HOLD} (pA)	Cm (pF)	R_{IN} (MΩ)	Tau (ms)	n
Control	-67.7 ± 1.9	-62.9 ± 26.3	367.41 ± 28.7	192.7 ± 16.5	36.8 ± 2.9	17/8/4
Thalamic Astrogliosis	-73.6 ± 2.1	-1.8 ± 18.1	340.3 ± 32.1	224.8 ± 22.1	32.7 ± 2.4	14/7/5
P-Value	**0.053**	0.1	0.57	0.32	0.31	
50 µM Picrotoxin	V_{REST} (mV)	I_{HOLD} (pA)	Cm (pF)	R_{IN} (MΩ)	Tau (ms)	n
Control	-68.3 ± 1.6	-195.8 ± 38.2	101.1 ± 10.0	290.1 ± 41.1	36.3 ± 7.3	9/5/3
Thalamic Astrogliosis	-68.7 ± 2.4	-196.3 ± 24.2	116.8 ± 7.3	208.3 ± 32.7	37.0 ± 5.3	13/9/5
P-Value	0.59	0.99	0.21	0.39	0.29	

Table S3. Passive electric membrane properties of thalamocortical neurons. Related to Fig. 3. Data represented as mean ± SEM, compared using Mann-Whitney U Test. Last column ("n") indicates the number of cells, slices, and mice (respectively) for each condition.

Table S4.

At -60 mV

	Rheobase (pA)	AP Amp. (mV)	AP Threshold (mV)	AP Duration (ms)	AP Half-Duration (ms)	n
Control	86 ± 17.9	67.3 ± 2.6	-55.4 ± 0.7	3.11 ± 0.84	1.35 ± 0.20	15/8/4
Thalamic Astrogliosis	100 ± 17.4	68.3 ± 1.3	-57.7 ± 0.5	2.08 ± 0.08	1.07 ± 0.04	14/7/5
P-Value	0.72	0.81	***0.022**	0.068	0.142	

At -75 mV

	Rheobase (pA)	AP Amp. (mV)	AP Threshold (mV)	AP Duration (ms)	AP Half-Duration (ms)	
Control	104.1 ± 11.5	69.6 ± 1.7	-57.0 ± 0.7	2.25 ± 0.08	1.15 ± 0.04	17/8/4
Thalamic Astrogliosis	91.4 ± 11.4	69.5 ± 1.1	-58.6 ± 0.6	1.93 ± 0.15	1.04 ± 0.04	14/7/5
P-Value	0.52	0.77	0.11	**0.052**	0.11	

At -60 mV

50 µM Picrotoxin	Rheobase (pA)	AP Amp. (mV)	AP Threshold (mV)	AP Duration (ms)	AP Half-Duration (ms)	n
Control	90 ± 35.5	68.2 ± 2.25	-51.7 ± 1.32	1.84 ± 0.09	0.89 ± 0.05	8/4/3
Thalamic Astrogliosis	70 ± 22	66.1 ± 3.86	-49.6 ± 1.21	2.38 ± 0.25	1.10 ± 0.04	5/5/2
P-Value	0.92	0.85	0.28	***0.018**	****0.0083**	

At -75 mV

50 µM Picrotoxin	Rheobase (pA)	AP Amp. (mV)	AP Threshold (mV)	AP Duration (ms)	AP Half-Duration (ms)	
Control	130 ± 33.5	68.5 ± 2.91	-52.6 ± 1.78	1.84 ± 0.09	0.93 ± 0.04	9/5/3
Thalamic Astrogliosis	151.5 ± 22.8	72.1 ± 1.91	-52.7 ± 0.87	2.07 ± 0.16	0.99 ± 0.05	13/9/5
P-Value	0.31	0.32	0.65	0.47	0.37	

Table S4. Active electric membrane properties of thalamocortical neurons. Related to Fig. 3. Data represented as mean ± SEM, compared using Mann-Whitney U Test. Last column ("n") indicates the number of cells, slices, and mice (respectively) for each condition. Action potential (AP). **P*<0.05, ***P*<0.01.

Table S5.

	Max. Area (pA*ms)	V_{50} (mV)	Max. Tau (ms)	Cm (pF)
Control	-21334 ± 2552	-113.20 ± 0.89	170.8 ± 37.4	96.64 ± 14.43
Thalamic Astrogliosis	-18178 ± 2929	-115.72 ± 0.85	268.3 ± 58.4	92.47 ± 9.57
P-Value	0.23	0.087	0.18	0.95

Table Continued	Max. Amp. (pA)	T-current Density (pA/pF)	Boltzmann Slope Factor	n
Control	-137.21 ± 21.4	-1.44 ± 0.15	-0.024 ± 0.002	6/6/3
Thalamic Astrogliosis	-112.80 ± 22.8	-1.31 ± 0.311	-0.029 ± 0.004	8/5/4
P-Value	0.41	0.35	0.57	

Table S5. T-Type Ca^{2+} current properties in thalamocortical neurons. Related to Fig. 3.
Data represented as mean ± SEM, compared using Mann-Whitney U Test. Last column ("n") indicates the number of cells, slices, and mice (respectively) for each condition.

Table S6.

Spontaneous Excitatory Post-Synaptic Currents (sEPSCs)						
	Frequency (Hz)	**Amplitude (pA)**	**Charge (fC)**	**Decay Tau (ms)**	**Rise Time (ms)**	**n**
Control	2.23 ± 0.72	17.77 ± 1.33	53.13 ± 4.15	2.18 ± 0.18	0.47 ± 0.05	15/9/4
Thalamic Astrogliosis	1.47 ± 0.33	16.19 ± 0.6	53.19 ± 4.42	2.31 ± 0.15	0.38 ± 0.03	16/8/5
P-Value	0.57	0.65	0.89	0.57	0.32	

Spontaneous Inhibitory Post-Synaptic Currents (sIPSCs)						
	Frequency (Hz)	**Amplitude (pA)**	**Charge (fC)**	**Decay Tau (ms)**	**Rise Time (ms)**	**n**
Control	4.98 ± 1.23	-27.09 ± 2.01	-292.1 ± 28.85	6.13 ± 0.40	2.35 ± 0.26	12/12/3
Thalamic Astrogliosis	3.17 ± 0.63	-32.86 ± 3.10	-394.1 ± 56.86	7.28 ± 0.64	3.12 ± 0.22	10/10/4
P-Value	0.54	0.2	0.16	0.16	****0.0085**	

Table S6. Spontaneous excitatory and inhibitory post-synaptic currents in thalamocortical neurons. Related to Fig. 3.

Data represented as mean ± SEM, compared using Mann-Whitney U test. Last column ("n") indicates the number of cells, slices, and mice (respectively) for each condition. $^{**}P<0.01$.

Table S7.

	V_{REST} (mV)	Cm (pF)	R_{IN} (MΩ)	Tau (ms)	n
Control	-65.68 ± 5.4	138.97 ± 27.7	495.9 ± 122.6	49.7 ± 9.5	7/5/3
Thalamic Astrogliosis	-64.52 ± 2.3	108.71 ± 10.5	411.2 ± 71.9	32.1 ± 4.9	13/7/4
P-Value	0.66	0.49	0.52	0.068	

50 uM Picro	V_{REST} (mV)	Cm (pF)	R_{IN} (MΩ)	Tau (ms)	n
Control	-56.97 ± 0.67	79.87 ± 7.22	526.5 ± 73.5	57.98 ± 7.65	16/8/3
Thalamic Astrogliosis	-55.98 ± 0.66	69.35 ± 6.13	487.12 ± 65.7	64.20 ± 13.36	22/9/4
P-Value	0.29	0.46	0.63	0.94	

	Rheobase (pA)	AP Amp. (mV)	AP Threshold (mV)	AP Duration (ms)	AP Half-Duration (ms)	n
Control	30.0 ± 10.3	43.64 ± 2.4	49.94 ± 1.53	1.30 ± 0.12	0.66 ± 0.07	7/5/3
Thalamic Astrogliosis	53.3 ± 14.7	47.7 ± 1.9	-52.91 ± 0.71	1.38 ± 0.06	0.67 ± 0.03	13/7/4
P-Value	0.34	0.24	0.097	0.4	0.28	

50 uM Picro	Rheobase (pA)	AP Amp. (mV)	AP Threshold (mV)	AP Duration (ms)	AP Half-Duration (ms)	n
Control	37.5 + 6.6	54.38 ± 1.33	-52.67 ± 0.79	1.15 ± 0.04	0.57 ± 0.02	16/8/3
Thalamic Astrogliosis	50.9 + 6.5	47.89 ± 1.77	-52.12 ± 0.84	1.25 ± 0.05	0.62 ± 0.03	22/9/4
P-Value	0.09	****0.0043**	0.69	0.25	0.29	

Table S7. Passive and active electrical membrane properties in reticular thalamic neurons. Related to Fig. 3. Cells were clamped at -75 mV. Data represented as mean ± SEM, compared using Mann-Whitney U Test. Last column ("n") indicates the number of cells, slices, and mice (respectively) for each condition. Action potential (AP). ***P*<0.01.

Table S8.

Spontaneous Excitatory Post-Synaptic Currents (sEPSCs)

	Frequency (Hz)	Amplitude (pA)	Charge (fC)	Decay Tau (ms)	Rise Time (ms)	Half Width (ms)	n
Control	4.06 ± 0.66	-25.11 ± 0.80	-28.82 ± 1.28	0.70 ± 0.04	0.50 ± 0.009	0.72 ± 0.03	15/8/3
Thalamic Astrogliosis	2.96 ± 0.33	-23.83 ± 0.68	-31.24 ± 1.53	0.80 ± 0.04	0.48 ± 0.01	0.79 ± 0.04	15/6/3
P-Value	0.27	0.25	0.25	0.09	0.062	0.072	

Spontaneous Inhibitory Post-Synaptic Currents (sIPSCs)

	Frequency (Hz)	Amplitude (pA)	Charge (fC)	Decay Tau (ms)	Rise Time (ms)	Half Width (ms)	n
Control	0.78 ± 0.22	-15.37 ± 0.81	-1720 ± 93	64.68 ± 5.86	5.07 ± 0.78	45.66 ± 5.06	10/6/5
Thalamic Astrogliosis	0.69 ± 0.21	-18.34 ± 2.73	-2044 ± 617	75.07 ± 11.35	6.22 ± 1.55	46.68 ± 9.31	8/6/4
P-Value	0.76	0.83	0.32	0.57	0.68	0.63	

Table S8. Spontaneous excitatory and inhibitory post-synaptic currents in reticular thalamic neurons. Related to Fig. 3.

Data represented as mean ± SEM, compared using Mann-Whitney U Test. Last column ("n") indicates the number of cells, slices, and mice (respectively) for each condition.

Table S9.

Frequency Band	Light Cycle		Dark Cycle	
	Control	Thalamic Astrogliosis	Control	Thalamic Astrogliosis
	n=6	n=6	n=6	n=6
Delta (1-4 Hz)	0.688	>0.99	0.844	0.844
Theta (4-8 Hz)	0.563	0.563	0.844	>0.99
Alpha (8-12 Hz)	0.844	0.156	>0.99	>0.99
Sigma (12-15 Hz)	0.563	***0.031**	0.844	0.219
Beta (15-30 Hz)	>0.99	0.156	0.688	0.063
Gamma (30-75 Hz)	>0.99	0.094	0.844	***0.031**
Total (1-75 Hz)	0.688	0.563	>0.99	0.563

Frequency Band	Light Cycle		Dark Cycle	
	Control +GAT-3	Thalamic Astrogliosis +GAT-3	Control +GAT-3	Thalamic Astrogliosis +GAT-3
	n=3	n=4	n=3	n=4
Delta (1-4 Hz)	0.25	0.375	0.57	0.875
Theta (4-8 Hz)	0.75	0.875	0.5	0.875
Alpha (8-12 Hz)	0.75	0.875	0.5	0.875
Sigma (12-15 Hz)	0.99	0.875	0.5	0.625
Beta (15-30 Hz)	0.5	0.875	0.5	0.875
Gamma (30-75 Hz)	0.5	0.875	0.5	0.875
Total (1-75 Hz)	0.5	0.875	0.5	0.875

Table S9. Comparison of S1 ECoG spectral features. Related to Fig. 6. Comparison of S1 ECoG power across different frequency bands, seven weeks following induction of thalamic astrogliosis. P-Values obtained from Wilcoxon matched-pairs signed rank test (non-parametric equivalent of paired t-test) between contralateral S1 and ipsilateral S1 in each group across different frequency bands. *$P<0.05$. Control: n=6 mice; Thalamic Astrogliosis: n=6 mice; Control+GAT-3: n=3 mice; Thalamic Astrogliosis+GAT-3: n=3 mice.

Table S10.

Data QC Measure	Sham	Stroke	TBI
Number of Spots Under Tissue	2,321	2,216	2,214
Mean Reads per Spot	71,181	112,417	161,322
Median Genes per Spot	4,870	5,080	5,326
Sequencing			
Number of Reads	165,211,061	249,115,248	357,166,098
Valid Barcodes	96.8%	96.7%	96.5%
Valid UMIs	100.0%	100.0%	100.0%
Sequencing Saturation	68.1%	76.4%	83.3%
Q30 Bases in Barcode	96.2%	96.3%	96.3%
Q30 Bases in RNA Read	94.7%	94.8%	94.2%
Q30 Bases in UMI	96.0%	96.2%	96.2%
Mapping			
Reads Mapped to Genome	92.9%	92.4%	95.6%
Reads Mapped Confidently to Genome	90.8%	90.1%	93.5%
Reads Mapped Confidently to Intergenic Regions	4.8%	5.4%	4.8%
Reads Mapped Confidently to Intronic Regions	2.7%	3.4%	3.5%
Reads Mapped Confidently to Exonic Regions	83.3%	81.3%	85.3%
Reads Mapped Confidently to Transcriptome	81.6%	79.6%	83.5%
Reads Mapped Antisense to Gene	0.9%	0.8%	0.8%
Spots			
Fraction Reads in Spots Under Tissue	93.0%	92.7%	92.5%
Mean Reads per Spot	71,181	112,417	161,322
Mean Reads Under Tissue per Spot	63,568	99,299	142,732
Median UMI Counts per Spot	15,797	16,812	18,341
Median Genes per Spot	4,870	5,080	5,326
Total Genes Detected	20,489	21,007	21,447

Table S10. Data quality control for 10x Visium spatial transcriptomics analysis of mouse brain after cortical injury. Related to Fig. 7. Data quality control for 10x Visium spatial transcriptomics of mice after cortical injury. n=1 hemisection for each condition.